Synthetic Aperture Radar (SAR) Data Simulation for Radar Backscatter Cross-section Retrieval

Thesis submitted to the Andhra University in partial fulfillment of the requirements for the award of

Master of Technology in Remote Sensing and Geographic Information Systems

Submitted by

Kimeera Tummala

Under the Supervision of

Mr. Ashutosh Kumar Jha
Scientist/Engineer 'SD'
Geoinformatics Department
Remote Sensing and Geoinformatics Group

Mr. Shashi Kumar
Scientist/Engineer 'SD'
Photogrammetry & Remote Sensing Department
Remote Sensing and Geoinformatics Group

Indian Institute of Remote Sensing, ISRO,
Dept. of Space, Govt. of India Dehradun – 248001
Uttarakhand, India

August, 2014

CERTIFICATE

This is to certify that this thesis work entitled — *Synthetic Aperture Radar (SAR) Data Simulation for Radar Backscatter Cross-section Retrieval* is submitted by Ms. Kimeera Tummala in partial fulfillment of the requirement for the award of *Master of Technology in Remote Sensing and GIS* by the Andhra University. The research work presented here in this thesis is an original work of the candidate and has been carried out in Geoinformatics Department under the guidance of Mr. Ashutosh Kumar Jha, Scientist/Engineer 'SD' and Mr. Shashi Kumar, Scientist/Engineer 'SD' at Indian Institute of Remote Sensing, ISRO, Dehradun, India.

Mr. Ashutosh Kumar Jha
Scientist/Engineer 'SD',
Geoinformatics Department,
Indian Institute of Remote Sensing,
Dehradun

Mr. Shashi Kumar
Scientist/Engineer 'SD',
Photogrammetry & Remote Sensing Department,
Indian Institute of Remote Sensing,
Dehradun

Dr. S. K. Srivastava
Head,
Geoinformatics Department,
Indian Institute of Remote Sensing,
Dehradun

Dr. S. K. Saha
Dean (Academics),
Indian Institute of Remote Sensing,
Dehradun

DISCLAIMER

This document describes work undertaken as part pf a program of study at the Indian Institute of Remote Sensing of Indian Space Research Organization, Department of Space, Government of India. All reviews and opinions expressed therein remain the sole responsibility of the author, and do not necessarily represent those of the Institute.

Acknowledgements

The course of this project has been a time of great professional experience and has been possible because of the environment provided by the Indian Institute of Remote Sensing. For this, and for the encouragement and inspiration they provided, I thank Dr. Y. V. N. Krishna Murthy, Director IIRS, Dr. S. P. S. Kushwaha, Head PPEG and Dr. S. K. Saha, Dean Academics.

I wish to express deep gratitude to Mr. Ashutosh Kumar Jha for being such an inspiring and encouraging guide throughout my project. His belief in the project was a great motivation for me. I would also like to express my sincere thanks to Mr. Shashi Kumar for patiently understanding the problems of the project. Their professional advice, suggestions and timely guidance helped refine the outcome. I am thankful to all the faculty of Geoinformatics Department, especially Dr. S. K. Srivastava, HOD, and Mr. P. L. N. Raju, Group Head RSGG for their constructive suggestions during intermediate reviews. A special note of gratitude to Mr. Janardhan for taking an interest in the project and helping me execute the hardware fabrication successfully.

I would like to thank Mrs. Shefali Agarwal, Course Director, M.Tech and Head, PRSD for the smooth conduct of the course and also for the timely suggestions that helped in producing a better thesis. Due thanks to Dr. Ajanta Goswami for making the stay at IIRS hostel a comfortable one. Thanks are also due to the CMA team for their assistance, and to the maintenance staff at IIRS for the comfortable stay here.

I am grateful to Dr.-Ing. Stefan Auer, TUM and Professor Kenneth C. Jezek, The Ohio State University, for their timely help and suggestions. A special thanks to Defence Electronics Applications Lab (DEAL), DRDO, Dehradun for letting me use their Millimeter wave laboratory and assisting me in testing my equipment.

Good friends remain for life. I am grateful to all my classmates for being such good support throughout. All of them have made my stay at IIRS enjoyable. I would especially like to mention Vivek and Soumya for being there for me through thick and thin. My friends from GID, Akansha, Parag and Vaibhav have been the reason the work environment was enjoyable.

Last but most importantly, a huge thanks to my family for being there for me and putting up with my tantrums. Without them I would never have been able to make it through till this stage.

Abstract

Using microwaves for remote sensing has revolutionized many fields like agriculture, urban planning, atmosphere studies, meteorology, hydrology, ocean studies and space technology. The ability of the microwaves to penetrate cloud cover, atmospheric constituents and even earth's surface has made this technology irreplaceable. Synthetic Aperture Radar technology has improved the quality of microwave data many folds. Spaceborne SAR sensors are now capable of distinguishing individual features on the surface of the Earth. Airborne sensors have even higher resolutions. Despite these obvious advantages, microwave data is used only by experts and scientists because of the difficulty in the interpretation of these images. SAR images have a lot of unexpected signatures and distortions due to tall features on the Earth. The microwave signals travel in the form of circular wavefronts. This property causes occlusions and shadow regions. All these aspects make it difficult to interpret the SAR images correctly. Simulation of SAR images is a technique which makes it easier to interpret these images. A simple simulation algorithm that uses Muhleman's backscatter model is studied and implemented in this project.

A radar system of low power and resolution is easy to build and also to implement as a Synthetic Aperture Radar. Such a system will not replace the high resolution sensors, but can be used to collect images in real time. It can give an idea of the backscatter of a particular scene and thus can be used to verify simulation algorithms. In this project, one such system is built to operate in S-band with a centre frequency of 2.4GHz. It has low power and low range capabilities, but can beautifully detect objects in its field of view, and can also be used to find their ranges and velocities. It was also used in the Synthetic Aperture mode by moving it equal distances in equal intervals of time.

Table of Contents

LIST OF FIGURES

LIST OF TABLES

1. INTRODUCTION

Radar (RAdio Detection And Ranging) technology was initially used to detect objects at a distance using radio waves, the part of the electromagnetic spectrum with wavelengths ranging from 1 millimeter to 100 kilometers. This region of the electromagnetic spectrum was first used to detect the presence and range of aircraft at a distance during World War II. The radio waves have since been used in many other areas like communication, navigation, medicine, weather monitoring, astronomy and remote sensing of earth's surface. The higher frequency end of the radio wave region of EM spectrum is called the Microwave region. It is this region that is used for remote sensing and earth observation. With the start of the satellite era in the 1960's, earth observation has made great leaps and every walk of life has benefited from the data collected by satellites. The advent of microwave sensors has further added to the quality of satellite data.

Radar imaging has become a very useful tool in earth observation during the past decade. The ability of microwave sensors to scan an area despite cloud-cover and absence of sunlight is a major advantage over the optical sensors. The sensitivity of microwaves to surface roughness, moisture content and target orientation is used to obtain comprehensive information about the target.

The basic operation of radar imaging includes a radar fixed to the side of an aircraft (in case of airborne radars) or a satellite (in case of space-borne radars). The transmitting antenna releases a pulse of energy in the direction perpendicular to the flight path. The relative intensities of the reflected energy waves received by the antenna are used to generate images of the terrain. Most of the imaging radars used today are monostatic radar systems, i.e., they have a single antenna for both transmitting and receiving the radar pulses. The EM waves reflected from objects at different ranges reach the radar antenna at different times. The differences in time and frequency of the reflected waves are used to form the final image of the scanned area.

The quality and the amount of detail in a radar image depend on two types of resolutions - range resolution and azimuth resolution. Range resolution determines the ability of the radar to distinguish between two objects closely separated in the range direction, i.e., the direction perpendicular to the flight direction. In simple terms, two closely spaced objects can be distinguished on a radar image if the reflected signals from these two objects reach the radar antenna at different times. The range resolution depends on the pulse width of the EM radiation. Similarly, the ability of the radar to distinguish between two objects closely separated in the azimuth direction, i.e., along the flight direction, is the azimuth resolution. When two closely spaced objects are in

the radar beam simultaneously, they cannot be distinguished by the radar as two separate objects. Hence, azimuth resolution depends on the beamwidth of the radar pulse; two objects can be distinguished from each other on the image if the separation between them is more than the radar beamwidth. The beam width in turn depends on the length of the antenna in the azimuth direction. Greater the length of the antenna, lesser is the beamwidth and finer the resolution. The equation that relates antenna length to azimuth resolution is:

$$r_{az} = R \times \frac{\lambda}{l_a} \tag{1.1}$$

where r_{az} is the azimuth resolution, R is the slant range, i.e., the distance of target from sensor, λ is the radar wavelength and l_a is the antenna length. The fraction $\frac{\lambda}{l_a}$ gives the radar beamwidth.

From equation 1.1 it is clear that at a particular wavelength, the azimuth resolution can be improved by increasing the length of the antenna. This gave rise to the concept of "Synthetic Aperture Radar" where a large antenna is synthesized by moving a small antenna along a straight line in the azimuth direction. As the sensor passes over a target, many pulses of EM radiation are transmitted and reflected back to the sensor. The phase and amplitude of the reflected signals are recorded and the individual signals are focused to create a synthetic aperture. The azimuth resolution of such radar is high in spite of a smaller antenna and lower wavelength. Greater the time interval over which the images are combined, larger is the synthetic aperture.

These advantages have resulted in the launch of a number of satellites with microwave sensors. Some such satellites are Radarsat-1&2, RISAT-1&2, TerraSAR-X and they have majorly contributed to earth observation by giving information about the motion of objects on the earth, elevation, changes in the surface conditions, etc.

1.1. Relevance of the project

Synthetic Aperture Radar technology has evolved a great deal over the past few years. Space-borne sensors like TerraSAR-X/TanDEM-X, COSMO-SkyMed and RISAT have been launched, that give a very high spatial resolutions of below 1m. Such high resolutions have made it possible to monitor individual objects on the surface of the earth. But, as microwaves are sensitive to surface moisture content, roughness of the target surface, relative geometry of target and sensor, the interpretation of object signatures on the SAR images becomes difficult. Two objects having similar geometries may produce very different signatures owing to differences in their surface compositions. Or, the same object may produce completely different signatures when its relative position with the sensor changes. Distortion effects like layover and

foreshortening further make it difficult to understand and interpret the SAR images. Simulation techniques help to better interpret the SAR images despite these variations and distortions.

Target recognition is another area where simulation techniques have been successfully applied. High resolution SAR images have made it possible to identify and monitor single objects on the earth. This has proved extremely useful in urban context to identify and extract different types of urban structures. SAR simulation can be used to create a database of the different urban structures, to be used in target recognition *(Chang, Chiang, and Chen 2011)*. Another aspect of SAR imaging that makes simulation necessary is the nature of reflection of microwave signals from different target objects. The Electromagnetic wave scattering mechanisms are sophisticated and hence difficult to analyze without the help of simulation.

SAR simulation takes into account all the sensor and target characteristics, their locations with respect to the earth, sensor motion, SAR parameters, radiometric and geometric properties of the target object, and the environmental factors. Using this information, the Radar Cross-Section of the target (RCS), sensor's orbital parameters, etc are calculated. A lot of work has been done on SAR simulation and a few simulators have also been developed. But, these simulators have certain limitations in terms of the frequency range over which they can work, and also the type of targets that they can be used for. Most of the simulators available work on the basis of frequency domain simulation. These simulators have little flexibility; they cannot be used for a wide range of targets, waveform frequencies and platform deviations. Different simulators cater to different types of targets, frequencies and applications. Time-domain simulation overcomes this limitation as it provides greater modularity, i.e., the same algorithm can be used for all types of targets, frequencies, polarizations, target orientations and platform deviations.

Though the satellite SAR systems have good resolution and are highly accurate, they cannot be used for in-situ measurements during field work or for empirical calculations on SAR signals in the laboratory. It can be used for testing simulation algorithms and developing processing techniques. An understanding of the internal working of SAR systems will pave the path for development of sensors with better resolution and efficiency. The working of SAR system in different frequency ranges can be studied by making small changes in the hardware.

So, through this project, a SAR simulation model is proposed that can simulate the radar back-scatter cross-sections for different types of scatterers and subsequently generate SAR images for the scatterers. A small radar system is designed with the aim of collecting and processing data that can be conveniently used for the verification of simulation algorithm, make changes in the algorithm to give better results, and also to

observe the changes in imagery due to changes in the sensor parameters. Space-borne SAR data like that from Radarsat-2 and ALOS PALSAR has been used to validate the simulation results.

1.2. Synthetic Aperture Radar basics

1.2.1. SAR Geometry

Figure 1.1 shows the imaging geometry of a space-borne Synthetic Aperture Radar.

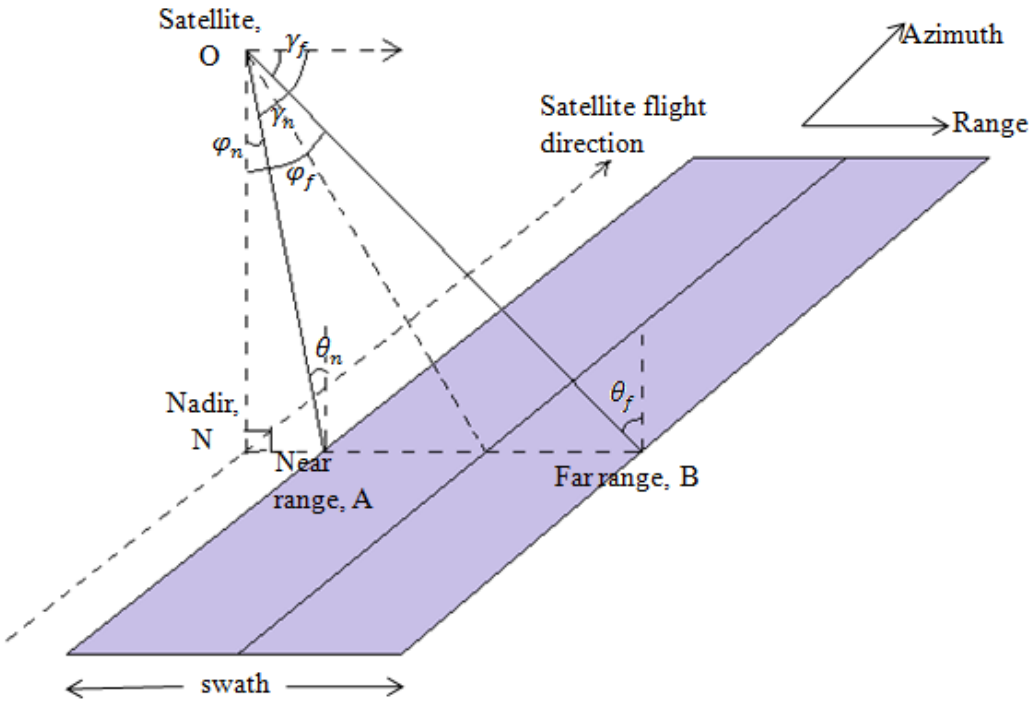

Figure. 1.1 SAR imaging geometry

In figure 1.1, the coloured portion represents the ground track being scanned by the sensor. 'A' and 'B' are points at near range and far range respectively. The direction parallel to flight path is called azimuth direction and that perpendicular to the flight path is called the range or look direction. The various terms and their definitions are given below *(Wolff, 1996)*.

1.2.1.1. Depression angle

It is the angle between the horizontal and the line joining the sensor to the point on the ground, i.e., the radar beam. In figure 1.1, γ_n and γ_f represent the near range and far range depression angles respectively. In the case of space-borne sensors, incidence angle which is the complement of depression angle is generally used.

1.2.1.2. Incidence angle

It is the angle between the radar beam and the normal vector to the earth. The value of incidence angle increases from near range to far range. This can be observed in figure 1.1, where θ_n is the near range incidence angle and θ_f is the far range incidence angle.

Earth's surface is almost never exactly flat. Hence, the normal vector to the earth is not same as the local surface normal. This led to the introduction of the term 'local incidence angle', which is defined as the angle between the radar beam and the local surface normal.

1.2.1.3. Look angle

It is the angle between the nadir line from the satellite to the ground and the radar beam. The angles φ_n and φ_f in figure 1.1 represent the near range and far range look angles respectively.

1.2.1.4. Slant range and ground range

The distance from the radar antenna on the satellite to the object being scanned is called the slant range. The distance OB in figure 1.1 is the slant range distance of an object at point B. The horizontal distance along the ground corresponding to the slant range is termed as the ground range. In the figure, ground range of an object at B is the distance NB. Hence, slant range and ground range can be related to each other as:

$$R_g = R \times \sin(look\ angle) \qquad \text{----(1.2)}$$

Or

$$R_g = \frac{R}{\cos(depression\ angle)} \qquad \text{----(1.3)}$$

where R_g is the ground range and R is the slant range.

1.3. Research objective

The main objective of the study is to retrieve radar backscatter cross-section for different types of features using SAR simulation modeling and to validate the simulation results using real SAR images.

1.4. Sub-objectives

- To generate SAR images using simulation technique
- To compare the simulated SAR images generated using DEMs of different resolutions
- To compare the simulated SAR images with real SAR images
- To design a radar system that can be implemented as a Synthetic Aperture Radar and collect SAR images on field

1.5. Research questions

The following research questions have been addressed in the course of the project work:

- What are the inputs and the procedure for the simulation of SAR images?
- What are the different parameters that contribute to the backscatter from a target and how are these parameters taken into consideration for simulation modeling?
- What are the design specifications for different sub-systems of a radar system?
- What is the accuracy of the simulation model with respect to the real SAR image?
- How is the RCS for complex features simulated?

1.6. Structure of the thesis

The thesis has been divided into five chapters. The first Chapter gives the overview of the research work, with introduction of the research, its relevance, research objectives and questions. The second chapter is a review of literature and summarizes various studies and techniques related to the present research. The methodology and data used for the project work are explained in the third chapter. The fourth chapter presents and discusses the results obtained. The Fifth chapter consists of the conclusions and recommendations.

2. REVIEW OF LITERATURE

SAR simulation has been an area of active research for a long time owing to its importance in data analysis, target recognition, satellite mission planning and sensor parameter optimization. The concepts involved in SAR simulation and the different techniques used in the simulation process have been studied extensively by a number of scientists. SAR signal simulation can be done in frequency domain or in time domain, each having its own advantages and disadvantages. While frequency domain analysis gives accurate results, it provides little flexibility as it can be used for only a small range of targets, waveform frequencies and platform velocities. Time domain analysis, on the other hand, provides greater modularity, works for a wide range of frequencies, but is computationally inefficient.

SAR simulation involves three major steps:

- Creation of 3D model of the target
- Computation of Radar Cross-Section of the target
- Range and azimuth compression to generate image, i.e., image focusing

2.1. 3D model of the target

A 3-dimensional model of the scene to be simulated is the first requirement of SAR image simulation. Digital Elevation Models, LiDAR-based elevation profiles, 3D models created using CAD, Google SketchUp, 3DS Max, etc. can be used to simulate SAR images. The amount of detail in a simulated SAR image depends on the amount of detail of the target 3D model.

2.2. Computation of Radar Cross-Section

Radar Cross-Section is the area a target would have to occupy to produce the amount of reflected power that is detected back at the radar. It depends on sensor viewing direction, frequency and polarization of radar signal, and geometry and surface properties of target *(Uluisik et al. 2008)***.** The prediction of RCS of a target is the most important aspect of SAR image simulation, as it determines the reflected signal intensity for the target at the sensor.

High-Frequency Asymptotic (HFA) techniques have been applied to predict RCS successfully. These techniques include Geometrical Optics, Physical Optics, Geometrical Theory of Diffraction, and Physical Theory of Diffraction. With the advent

of high-speed personal computers with parallel processing capabilities, pure numerical methods like Finite Difference Time Domain (FDTD) method, Method of Moments (MoM), Fast Multipole Method (FMM) and Transmission-Line Matrix (TLM) technique have gained importance. These numerical methods can be used for any target irrespective of geometry and computational limitations *(Uluisik et al. 2008)*.

Geometrical Optics or Ray Optics considers the propagation of Electromagnetic Radiation in the form of rays. Ray tracing is one method which uses Ray Optics to calculate the intensity contribution of a point on the target *(S. Auer, Hinz, and Bamler 2010)*. This technique is widely used to render coloured images of scenes as imaged by an optical imaging device like a camera. The ray tracing algorithm traces light backwards from the observer to the light source. At each interaction of light with an object surface, the illumination is computed. Ray tracing uses the facts that radiance remains constant along a line of sight, and that the light scattering at surfaces is symmetric *(Jensen 2001)*. Ray tracing is integrated with reflection models to compute the intensity contributions of different points on the target objects. As this technique approximates EM waves to discrete rays, it does not account for various wave effects like polarization. Despite this drawback, ray tracing is considered one of the standard techniques used by various software systems for SAR simulation *(Hammer et al. 2008)*.

Physical Optics is a wave approximation for short wavelengths. It integrates the results obtained through ray optics over a surface, and thus accounts for certain wave properties of the EM radiation. Neither Geometrical Optics nor Physical Optics is accurate near edges and shadow boundaries, as they do not account for diffraction effects. The Geometrical Theory of Diffraction (GTD) and Physical Theory of Diffraction (PTD) are extensions of Geometrical Optics and Physical Optics respectively. They predict the second- and third-order scattering contributions made by diffracted rays *(Uluisik et al. 2008)*.

Finite Distance Time Domain (FDTD) method is a powerful, yet simple, numerical method for solving a system of differential equations, and has been applied to various phenomena including the calculation of Radar Cross-Section (RCS). It falls under the category of resonance category techniques, i.e., those in which the object particle size is comparable to the wavelength of the EM radiation. It uses finite differences to approximate spatial and temporal derivatives and can solve a wide range of problems, including the target RCS computations *(Schneider 2010)*.

FDTD is a computationally expensive and time-consuming method, and parallel processing at both hardware and software levels is done to make the model more efficient *(Cakir, Cakir, and Sevgi 2008)*. The target model and source are placed in the 3D FDTD volume, and electric and magnetic field components are calculated in this volume using the iterative FDTD equations. Near-to-Far-Field Transformation (NTFFT)

is applied to calculate the components at fields farther from the source. It involves the extrapolation of the near fields along a number of directions using surface electric and magnetic currents. Parallelization has been introduced for the application of NTFFT. The transformations for all the six faces of the virtual closed surface are done in parallel, thus efficiently reducing the time of implementation of the algorithm *(Çakır, Çakır, and Sevgi 2014)*.

Method of Moments (MoM) is a frequency domain method which uses a discrete-mesh model of the target. Each wire in the mesh is associated with a command called Generate Wire (GW) which contains the label and end points for that wire. This method solves the electric and magnetic field equations in their matrix form *(Uluisik et al. 2008)*.

2.3. Some prominent works

SARAS is a Synthetic Aperture Radar raw signal simulator developed by *Franceschetti et al. 1992*, where the frequency domain technique of Fast Fourier Transforms (FFT) was used for processing data. They presented a statistical model to simulate SAR raw data of a 3-dimensional scene using a facet model for the scene. In the facet model, the entire scene is locally approximated to facets instead of considering individual point scatterers. A tradeoff between resolution and memory requirement was achieved by using two-stage FFT algorithm. The simulator takes into consideration the terrain altitude, layover and shadow effects, SAR system aberrations, surface electromagnetic properties and frequency and polarization of transmit signal. The number of facets in the facet model can be increased to give a more detailed image, but this increases the computational and memory requirements. The SAR Raw Signal Simulator has been used to study and analyze high resolution SAR images of urban areas *(Franceschetti et al. 2007)*. The major backdrop of this model is that it restricts the simulator to surface scattering and does not work for multiple scattering.

Urban feature extraction, change detection and modeling are some areas where SAR simulation technique is most widely used. The high buildings and other structures on urban areas cause distortions due to occlusions in SAR images, thus deteriorating the quality of change detection. SAR simulation and comparison with real SAR images has been used to negate the effects of these distortions *(Balz 2004)*. Simulation is extremely useful when can be done in real-time to test different scenarios to avoid occlusions and distortions due to urban features. Such real-time applications have been developed using modern Graphical Processing Units (GPUs) which speed up the simulation process *(Balz and Haala 2006)*.

Another very important study in the field of SAR image simulation was done by *Chang, Chiang, and Chen 2011*. They developed a technique to simulate SAR images with the

specific aim of using the simulated images for target recognition. The algorithm used to calculate the Radar Cross-Section (RCS) is the Radar Cross Section Analysis and Visualization System (RAVIS), which uses physical optics, physical diffraction theory and shooting and bouncing rays. The first two concepts, i.e., the physical optics and physical diffraction theory are used to compute the effects of single bounce scattering. The Shooting and Bouncing Rays algorithm is used to account for the multiple reflections. The target models used are 3D CAD models containing numerous polygons, each polygon associated with the RCS as a function of radar parameters and incident angle. The next step of image simulation, i.e., image focusing is done with the help of Range Doppler algorithm. Image focusing is a process where range compression is done on the basis of doppler centroid estimation. Further, azimuth compression is done to match the resolution of the simulated image to that of the SAR sensor used. The images simulated using these techniques have been successfully used to create a database to assist in target recognition, a few minor drawbacks being the inability of the algorithm to accommodate fully polarimetric data and to simulate very high resolution SAR images.

Ray tracing technique has been effectively used to develop a simulator RaySAR that can simulate high resolution SAR images *(S. Auer, Hinz, and Bamler 2010)(S. J. Auer 2011)*. The multiple reflections of electromagnetic waves are followed backwards from the receiver to the transmitter within the object scene. At each energy-matter interaction, the amount of radiation reflected in the direction of the ray is computed on the basis of the physical laws of reflection. The simulation algorithm discussed is implemented by modifying the source code of the rendering software POV Ray, which uses Constructive Solid Geometry (CSG) to define the scene geometry. The sensor is defined in the scene by means of a cylindrical light source emitting parallel rays for the transmission, and an orthographic sensor for the receiver. The intensity values at object surfaces are evaluated using different models for specular and diffuse reflections. Diffuse reflection is modeled on the basis of Lambert's law which states that "the radiant intensity observed from an ideal diffuse radiator is directly proportional to the cosine of the angle between the observer's line of sight and the surface normal". For specular reflection, the Fresnel reflection model is extended to incorporate specular highlight and also the diffuse components of fairly high intensity. Range and azimuth coordinates of a point are calculated on the basis of the number of bounces corresponding to that point and the distance travelled by the corresponding ray. Finally, an image with a regular grid is created from the irregularly distributed intensity contributions. The irregularity is a result of the side-looking imaging geometry of the SAR sensor. RaySAR could successfully simulate single and multiple-bounce effects and could also create high resolution images. The geometrical quality obtained through this simulation algorithm can be increased by increasing the level of detail of object models and the sampling density. But, the radiometric quality is low due to the use of specular and diffuse

reflection models that approximate the reflection processes. The radiometric detail is low also because discrete rays of Electromagnetic radiation are modeled instead of continuous waves.

SAR image simulation using Digital Elevation Model (DEM) as the target model has numerous applications like terrain mapping, positional and geometric correction in topographic maps, etc. For each DEM cell, the position of the corresponding image pixel is calculated in the slant range geometry. This position is in the form of row and column numbers in the image. Then the backscattered power is calculated for each pixel on the basis of a backscatter model *(Liu, Zhao, and Jezek 2004)*. Doppler centroid frequency is calculated and equated to the doppler shift to evaluate the instant of imaging of that particular DEM cell. This time instant is then used to calculate the row number of the DEM cell in the image. The range of each DEM cell from the sensor is used to find its column number in the image. In the next step, modified Muhleman's backscatter model is used to find the backscattered power at each pixel. The Muhleman's model is based on geometrical optics and depends on the surface slope and the local incidence angle *(Storvold et al. 2004)*.

2.4. Radar system design

Small scale radar systems have been used to conduct laboratory experiments, because the design is simple and the systems are extremely useful for empirical calculations. They are practical for testing and improving simulation algorithms. The parameters needed to be considered while designing a SAR system have been discussed. The microwave circuit theory has been explained in many books and technical papers *(Fuentes 2008) (Lathi 1998) (Mishra 2001)* which have helped in understanding the concepts involved in the design process . The Massachusetts Institute of Technology's web resource was a very useful source of information on the design of a SAR system and subsequent processing of the data collected *(Charvat G. L. 2011)*.

3. STUDY AREA AND DATA USED

3.1. Study area

SAR images from two satellites – RADARSAT-2 and ALOS PALSAR have been used to validate the simulation algorithm. The RADARSAT-2 image covers San Francisco area of the Unites States of America. This area is shown in figure 3.1.

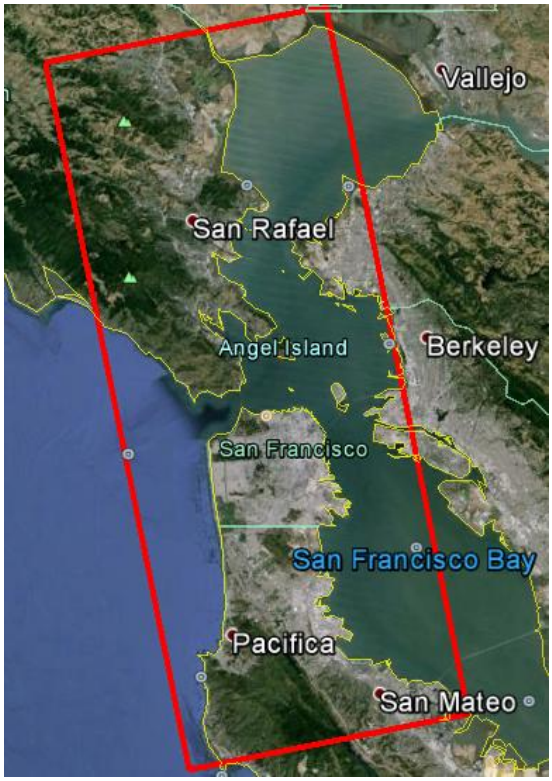

Figure 3.1: San Francisco area (Source: Google Earth)

The ALOS PALSAR data covers a part of Uttarakhand, India. The area covered by the ALOS PALSAR image is shown in figure 3.2.

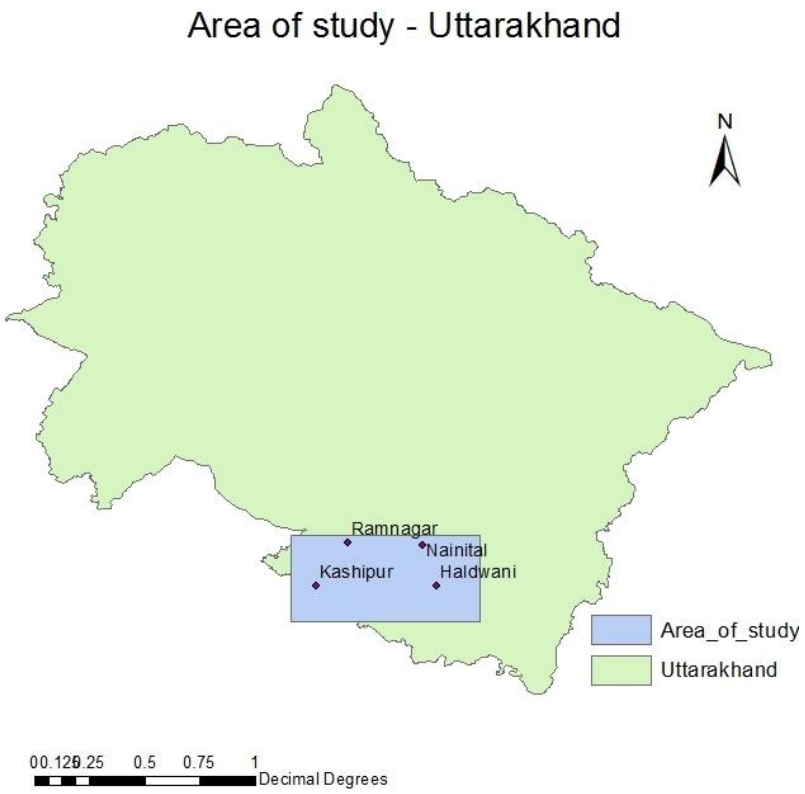

Figure 3.2: Part of Uttarakhand covered by ALOS PALSAR image

3.2. Data used

3.2.1 Digital Elevation Models (DEMs)

ASTER (Advanced Spaceborne Thermal Emission and Reflection Radiometer) DEM of spatial resolution 1 arc-second (30 m) and SRTM (Shuttle Radar Topography Mission) DEM of spatial resolution 3 arc-seconds (90 m) have been used in the project. Aster DEM (Japan Aerospace Exploration Agency 2009)has been downloaded from http://gdem.ersdac.jspacesystems.or.jp/. SRTM DEM has been downloaded from http://earthexplorer.usgs.gov/.

3.2.2. Satellite data

The data of RADARSAT-2 and ALOS PALSAR have been used to validate simulation results. Launched on 14 December 2007, RADARSAT-2 works in the C-band with a centre frequency of 5.4GHz, and has quad-polarization capability. It has a very high

resolution of 1m in the range direction and 3m in the azimuth direction in the spotlight mode. The orbit of RADARSAT-2 has an altitude of 798km and an inclination of 98.60^0. In this project, the Fine Quad scanning mode data of RADARSAT-2 is used. The properties of this mode are given in the table 3.1 *(Slade 2013)*.

Table 3.1: Specifications of Radarsat-2 Fine Quad-pol Mode

Swath width	25 km
Range resolution	5.2 - 16.5 m
Azimuth resolution	7.6 m
Incidence angle	18^0 - 49^0
Polarization	Quad-pol

Launched on 24 January 2006, ALOS PALSAR operates in the L-band with a centre frequency of 1.27GHz, and has quad-polarization capability. In fine mode, it has a range resolution of up to 7m. PALSAR products are available at different levels of processing – level 1.0, level 1.1 and level1.5. In the present study, PALSAR data of 1.1 processing level is used. This data is range compressed, single-look azimuth compressed and is on slant range coordinates *(Japan Aerospace Exploration Agency 2009)*. The metadata of these satellite images have been used in the simulation process.

3.3. Software used

ArcGIS 10 and ERDAS IMAGINE 2013 were used to process the Digital Elevation Models. MATLAB and R software environments were used to implement the simulation algorithm. Python language was used for the extraction of information from metadata of satellite images.

Multisim simulation software was used to simulate the power supply and modulator circuits of the radar system.

4. METHODOLOGY

4.1. SAR Simulation

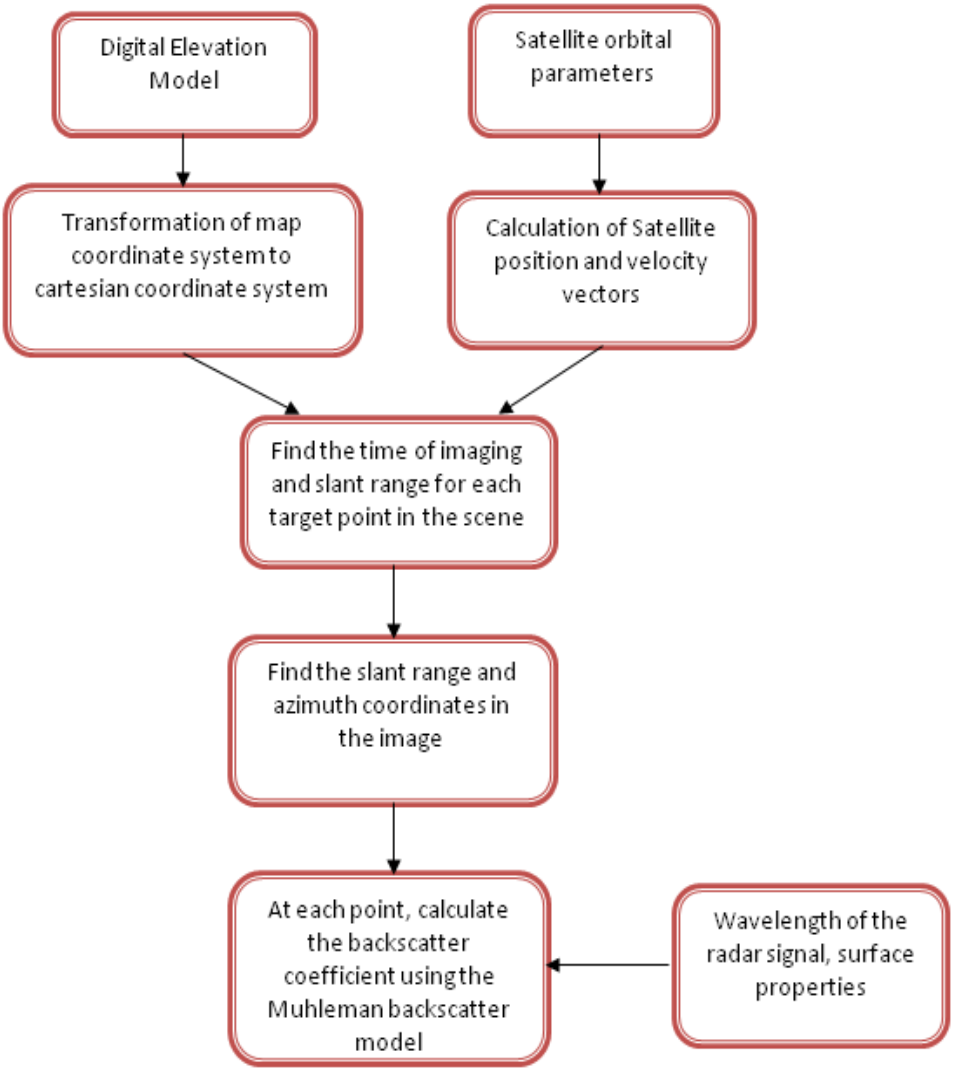

Figure 4.1: Methodology flow for SAR simulation

4.1.1. Processing of Digital Elevation Model

The Digital Elevation Model (DEM) acts as the 3D model of the target that is being simulated. DEM is a raster product that has elevation information at each pixel. This

information is converted into a matrix containing three columns - latitude, longitude and elevation. This is done by sample extraction in ArcGIS 10.

Both ASTER DEM and SRTM DEM are projected using WGS84 datum and UTM projection system. Hence, the coordinates of each pixel conform to geodetic coordinate system which has its center at the Earth's center of mass and a reference ellipsoid with respect to which all altitudes are measured **(reference - book)**. In order to reconstruct the Synthetic Aperture Radar imaging geometry, the DEM is transformed from geodetic coordinate system to a Cartesian coordinate system called the Earth Centered Earth Fixed (ECEF) coordinate system. The transformation is done by solving the following non-linear equations:

$$\begin{bmatrix} X \\ Y \\ Z \end{bmatrix} = \begin{bmatrix} (N+h)\cos(lat)\cos(lon) \\ (N+h)\cos(lat)\sin(lon) \\ \{(1-e^2)N+h\}\sin lat \end{bmatrix} \quad (4.1)$$

where X, Y, Z are the Cartesian coordinates; 'h' is the altitude of the point in metres; 'lat' and 'lon' are the latitude and longitude of the point respectively, in degrees; 'e' is the eccentricity ellipsoid; 'N' is the radius of curvature in prime vertical. 'N' and 'e' are given by

$$e = \sqrt{1 - \frac{b^2}{a^2}} \quad (4.2)$$

$$N = \frac{a}{\sqrt{1-e^2 sin^2(lat)}} \quad (4.3)$$

where 'a' and 'b' are semi-major axis and semi-minor axis of the ellipsoid respectively *(Ligas and Banasik 2011)*. For WGS84 datum used here, the semi-major axis is 63,78,137 mans semi-minor axis is 63,56,752.3142 m. Table 4.1 shows the list of points extracted from the DEM. The first column consists of latitudes in degrees, the seconds consists of longitudes in degrees, and the third has altitudes values in metres. Table 4.2 shows the list of the same DEM points in ECEF coordinate system after performing the transformation using equation 4.1 to 4.3.

Table 4.1 : Latitude (in degrees), longitude(in degrees), altitude (in metres) extracted from DEM

38.11045	-122.694	250
38.11045	-122.693	247
38.11045	-122.693	242
38.11045	-122.693	235
38.11045	-122.692	228
38.11045	-122.692	222
38.11045	-122.692	218
38.11045	-122.692	214
38.11045	-122.691	211
38.11045	-122.691	209

Table 4.2 : DEM points in cartesian coordinates(X,Y,Z) after transformation

-2.71E+06	-4.23E+06	3.92E+06
-2.71E+06	-4.23E+06	3.92E+06
-2.71E+06	-4.23E+06	3.92E+06
-2.71E+06	-4.23E+06	3.92E+06
-2.71E+06	-4.23E+06	3.92E+06
-2.71E+06	-4.23E+06	3.92E+06
-2.71E+06	-4.23E+06	3.92E+06
-2.71E+06	-4.23E+06	3.92E+06
-2.71E+06	-4.23E+06	3.92E+06
-2.71E+06	-4.23E+06	3.92E+06

4.1.2. Extraction of information from satellite metadata

The next step in the simulation process is to find the SAR sensor's position and velocity vectors with respect to time. This can be done in two ways. The first method is by using the Two Line Element (TLE) datasets which contain the orbital information of the sensor. They are available on the internet (http://www.celestrak.com/NORAD/elements/). The TLE dataset for each satellite has three lines - Line 0, Line 1 and Line 2. Line 0 consists of 24 characters which represent the name of the satellite. Line 1 and Line 2 have 69 characters (including blank spaces) each. A sample TLE set for RADARSAT-2 is given below.

RADARSAT-2
1 32382U 07061A 14015.49108034 .00000123 00000-0 64681-4 0 6871
2 32382 98.5762 25.2155 0001193 85.2031 77.0625 14.29985288317835

The description of the TLE datasets is given in tables 3.4 and 3.5.

Table 4.3: Description of Two Line Element dataset - Line1

Line 1	
Column	**Description**
01	Line Number of Element Data
03-07	Satellite Number
08	Classification (U=Unclassified)
10-11	International Designator (Last two digits of launch year)
12-14	International Designator (Launch number of the year)
15-17	International Designator (Piece of the launch)
19-20	Epoch Year (Last two digits of year)
21-32	Epoch (Day of the year and fractional portion of the day)
34-43	First Time Derivative of the Mean Motion
45-52	Second Time Derivative of Mean Motion (decimal point assumed)
54-61	BSTAR drag term (decimal point assumed)
63	Ephemeris type
65-68	Element number
69	Checksum (Modulo 10) (Letters, blanks, periods, plus signs = 0; minus signs = 1)

Table 4.4: Description of Two Line Element dataset - Line2

Line 2	
Column	**Description**
01	Line Number of Element Data
03-07	Satellite Number
09-16	Inclination [Degrees]
18-25	Right Ascension of the Ascending Node [Degrees]
27-33	Eccentricity (decimal point assumed)
35-42	Argument of Perigee [Degrees]
44-51	Mean Anomaly [Degrees]
53-63	Mean Motion [Revs per day]
64-68	Revolution number at epoch [Revs]
69	Checksum (Modulo 10)

Source: http://www.celestrak.com/NORAD/documentation/tle-fmt.asp

The TLE datasets give the six orbital parameters which describe the orbit of the satellite in space. These parameters, called the Keplerian orbit elements are:

- Semi-major axis, a
- Eccentricity, e
- Argument of periapsis, ω
- Longitude of Ascending Node (LAN), Ω
- Inclination, i
- Mean anomaly M_0 at epoch t_0

The steps for the determination of position and velocity vectors of the satellite from Keplerian orbital parameters are *(Eng and Schwarz 2013)*:

i. Find eccentric anomaly E(t) by solving Kepler's equation

$$M(t) = E(t) - e \sin E \quad (4.4)$$

ii. Find the true anomaly ν(t)

$$\mathrm{v(t)} = 2.\arctan2(\sqrt{1+e}\sin\frac{E(t)}{2}, \sqrt{1+e}\cos\frac{E(t)}{2} \quad (4.5)$$

iii. Find the distance to the central body

$$r_c(t) = a(1 - e\cos E(t)) \quad (4.6)$$

iv. Determine the position and velocity vectors

$$Position\ vector, S(t) = \begin{bmatrix}\cos \mathrm{v(t)} \\ \sin \mathrm{v(t)} \\ 0\end{bmatrix} \quad (4.7)$$

$$Velocity\ vector, V_s(t) = \frac{\sqrt{\mu a}}{r_c(t)}\begin{bmatrix}-\sin E \\ \sqrt{1-e^2}\cos E \\ 0\end{bmatrix} \quad (4.8)$$

The other method is by extracting the instantaneous positions and velocities of satellite from its metadata and using this data to fit equations representing position and velocity vectors. In this thesis, this method is adopted. The metadata of RADARSAT-2 is in the form of an Extensible Markup Language (XML) document which contains the details of radar parameters like its frequency, polarization, pulse bandwidth, pulse repetition frequency, etc. It contains the satellite orbit and attitude parameters, the coordinates of the satellite at different positions during the imaging of the scene, its velocity at those positions, and its attitude (yaw, roll and pitch) at those positions. It contains image generation parameters, SAR processing information including Doppler centroid information, number of range and azimuth looks and slant range to ground range conversion coefficients. The metadata also contains image attributes like number of lines, number of samples per line, and image and geodetic coordinates of the points. The geodetic coordinates include latitude and longitude in degrees and height in metres.

The metadata of RADARSAT-2 image used in the present study has the position and velocity information at five instants during the imaging of the scene. These five positions and velocities at these positions are extracted through Python scripting. The position and velocity vectors are then determined using the Newton-Raphson curve fitting method. The satellite position and velocity thus extracted are then transformed from Earth Centered Inertial to Earth Centered Earth Fixed coordinate system.

4.1.3. Calculation of SAR image coordinates for DEM cells

In order to determine the row and column number of a DEM cell in the SAR image, its range from the SAR sensor and its time of imaging must first be calculated. The range of a DEM cell from the sensor is calculated by the simple Euclidean distance formula as follows:

$$R(t) = \sqrt{\big(S(t) - P(t)\big).\big(S(t) - P(t)\big)} \qquad (4.9)$$

where S(t) is the satellite position vector and P(t) is the position of DEM cell. Time of imaging, 't' for each DEM cell is found by solving the Doppler equation. The Doppler frequency shift due to the motion of the SAR sensor is given by:

$$f_D(t) = \frac{2}{\lambda R(t)}\Big(V_s(t) - V_p(t)\Big).\big(S(t) - P(t)\big) \qquad (4.10)$$

where $V_s(t)$ is the sensor velocity vector, $V_p(t)$ is the target velocity vector and λ is the radar wavelength. The target velocity $V_p(t)$ is due to the earth's rotation, and is given by

$$V_p = \omega_E \times P \qquad (4.11)$$

where ω_E is the angular velocity of Earth's rotation *(Liu, Zhao, and Jezek 2004)*.

The Doppler centroid frequency is given by the formula

$$f_{DC} = \frac{2\,|V_s - V_p|}{\lambda}\sin\tau \qquad (4.12)$$

where τ is the squint angle, i.e., the angle between the line joining sensor to the DEM cell and zero Doppler plane. The average squint angle for RADARSAT-2 is 2.826^0 ($\pm 0.011^0$) *(Chiu and Livingstone 2005)*.

At the instant when the Doppler centroid frequency equals the Doppler frequency shift, the radar beam intersects the corresponding pixel on the DEM. That instant is the time of imaging of that DEM cell. To find the time of imaging 't', the following non-linear equation is solved using the Newton-Raphson method.

$$f_D(t) - f_{DC} = 0 \;\; i.e., \frac{2}{\lambda R(t)}\Big(V_s(t) - V_p(t)\Big).\big(S(t) - P(t)\big) - f_{DC} = 0 \qquad (4.13)$$

Once the time of imaging 't' is calculated for each DEM cell, its row number in the slant range image is given by

$$i = \frac{t - t_{offset}}{\delta t} \tag{4.14}$$

where t_{offset} is the time of first line and δt is the time between adjacent lines, both of which are obtained from the product metadata.

The column number of the DEM cell in the slant range image is given by

$$j = \frac{R - R_{offset}}{\delta R} \tag{4.15}$$

where R_{offset} is the range of first sample and δR is the spacing between adjacent pixels.

4.1.4. Determination of local incidence angles for DEM cells

The local incidence angle θ for each DEM cell is unique and depends on the surface slope at that point. This angle plays a major role in determining the amount and direction of backscatter from that DEM cell, thus contributing to the DEM cell's intensity in the SAR image. In this study, the local incidence angle is calculated from the slope and aspect of the DEM. If 'a' is the azimuth direction and 'r' is the range direction, then the slope in azimuth and range directions are calculated as s_x and s_y respectively. The unit vector in the direction of line joining SAR sensor to DEM cell is $\bar{r} = (r_x, r_y, r_z)$ and unit vector in the direction of surface normal at the DEM cell is $\bar{n} = (-s_x, -s_y, 1)$. Then,

$$\cos\theta = \bar{r}.\bar{n} \tag{4.16}$$

4.1.5. Calculation of backscattered intensity

The final step in the simulation of SAR images is to calculate the backscattered intensity from each DEM cell. The total intensity in a SAR image is a combination of both system and terrain effects *(Curlander and McDonough 1991)*. System effects include characteristics like polarization whixh are constant. The terrain effect is represented as the backscatter coefficient. For this, the Muhleman's backscatter model is used. According to this model, the backscatter is given by

$$\sigma = log_{10}\left(\frac{M^3 \cos\theta}{(\sin\theta + M\cos\theta)^3}\right) \tag{4.17}$$

where M is Muhleman's constant that depends on the average terrain slope. A modified form of Muhleman's model, with empirically determined constants is used in this project *(Storvold et al. 2004)*. The modified Muhleman's model is

$$\sigma = log_{10}\left(\frac{0.0133\cos\theta}{(\sin\theta + 0.1\cos\theta)^3}\right) \quad (4.18)$$

The backscatter at each pixel is calculated using equation (3.18). Now, the row number, column number and intensity value of each pixel has been determined. The image generated using these values is the simulated SAR image.

4.2. Design and building of radar system

A radar system of low power is built to assist in collecting field information. It is designed to operate in S band with a centre frequency of 2.4GHz. The radar system is a Frequency-Modulated Continuous-Wave (FMCW) radar which transmits a continuous wave of known stable frequency which is varied using a triangular modulating signal. Any radar system has three main parts: the transmit circuit, the receive circuit and the antennas. The transmit circuit consists of the circuitry which generates the Radio Frequency (RF) signal in the required bandwidth. The receive circuit consists of the circuitry which receives the reflected signal from the receiver antenna and compares it with the transmit signal. A signal with frequency equal to the difference of transmit and receive signals is generated by the receiver circuit. This mixed signal is then processed to obtain useful information from the radar.

Antennas are the devices which convert electrical power into RF signals, and vice versa. Radar signals are transmitted by the receiver antenna, get reflected by target objects, and are received by the receiver antenna. Radar systems that use two different antennas placed at a considerable distance from each other for transmitting and receiving radar signals are called bistatic radars and those that use the same antenna for both transmitting and receiving are called monostatic radars. Most spaceborne SAR systems are monostatic. In this project, two different antennas are used transmitting and receiving radar signals, but they are placed so close together that they act as a single antenna, hence making it a monostatic radar. The overall block diagram of the radar system is given in figure 3.3.

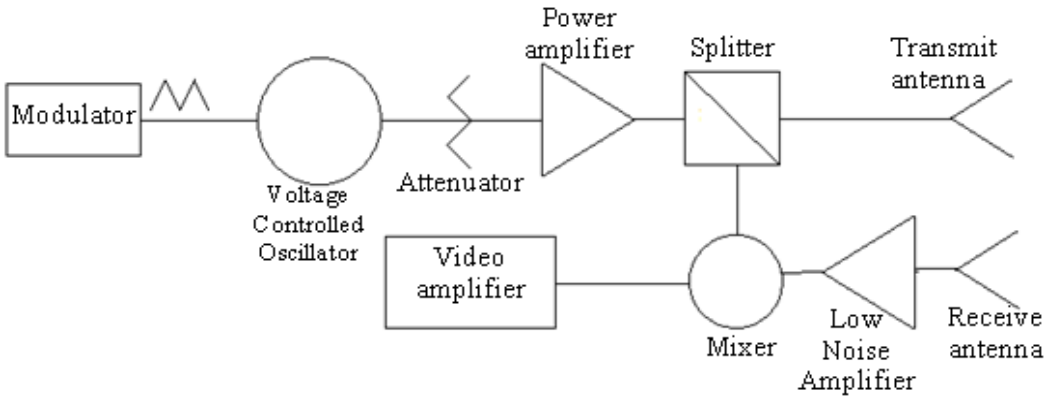

Figure 4.2: Block diagram of radar system *(Charvat G. L. 2011)*

4.2.1. Transmit circuit

The modulator, Voltage Controlled Oscillator, Attenuator, Power Amplifier and splitter make up the transmit circuit. Each of these components is explained in the following sections.

4.2.1.1. Modulator

The modulator circuit is used to generate a triangular waveform used to modulate the radar signal. It uses a function generator chip XR2206 to generate the triangular wave. It is a 16-pin IC with the capability to produce square and triangular waveforms. The pin description and electrical characteristics of XR2206 are given in Appendix. The electrical connections of XR2206 to obtain a triangular wave of frequency 25Hz, time period of 40ms (with rise time and fall time of 20ms each) and voltage in the range of 2 – 3.2V, are given in figure 3.4. These specifications of triangular waveform are determined by characterizing the Voltage Controlled Oscillator (VCO) which is modulated by the triangular wave generated by the modulator. The characterization of VCO is given in the next section.

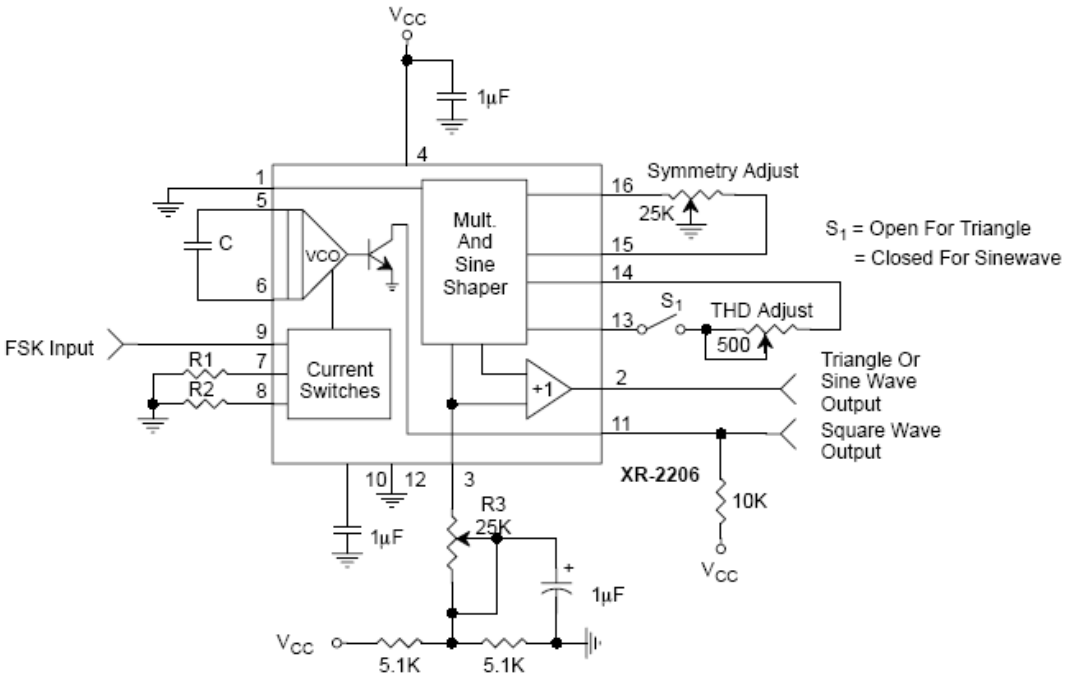

Figure 4.3: XR2206 connections (Source: Datasheet of XR2206 http://www.alldatasheet.com/datasheetpdf/pdf/80496/EXAR/XR2206.html)

In the present design, a variable resistor is used as the timing resistor R1 at pin 7. The value of this resistance is varied until a waveform of the required frequency is obtained at pin 2. The value of timing capacitance C is 0.47µF.

4.2.1.2. Voltage Controlled Oscillator (VCO)

VCO is a device whose oscillation frequency varies with respect to an input voltage called the modulating voltage or tuning voltage. The VCO selected for this design is ZX95-2536C+, which has a frequency range of 2315-2536 MHz. Its electrical specifications are given in Appendix. The tuning voltage (V_{tun}) vs. frequency plot of the VCO is done using a handheld RF Combination Analyzer (Agilent's N9914A, 6.5GHz).

Figure 4.4: Agilent RF analyzer

The readings of the RF analyzer are tabulated (table 4.5).

Table 4.5: V_{tun} and frequency readings of VCO

V_{tun} (volts)	Frequency (MHz)
0	2255
0.5	2297.5
1	2332.5
1.5	2367.5
2	2405
2.5	2440
3	2475
3.5	2510
4	2545
4.5	2565
5	2590

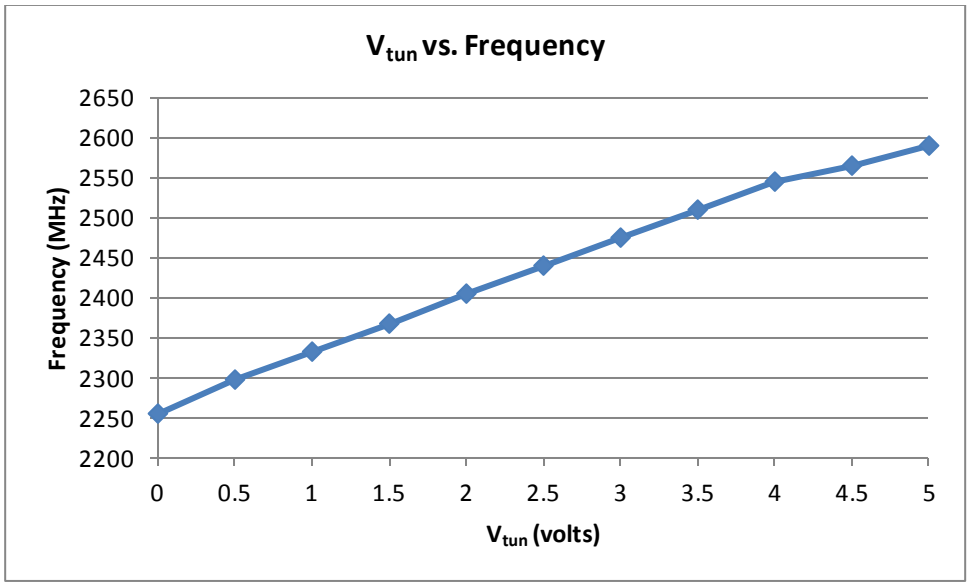

Figure 4.5: V_{tun} vs. Frequency characteristic of VCO

From the above characteristic, it is clear that for an operating frequency of 2400 MHz, the modulator needs to produce a tuning voltage waveform of approximately 2V. At this frequency, the VCO has an RF power output of 6dBm.

4.2.1.3. Attenuator and Power Amplifier

An attenuator is a passive device which reduces the gain of a system. This is required to reduce the Voltage Standing Wave Ratio (VSWR) due to the amplifier and the antenna. An amplifier connected in a circuit has impedance different from the transmission line. Because of this, some of the power flowing from the transmission line to the amplifier gets reflected back by the amplifier. In the circuit, the incoming power and reflected power form a standing wave, resulting in peaks and valleys as in a sine wave. In such a standing wave, the ratio of maximum value of voltage to the minimum value is called VSWR. If there is high amount of mismatch in the impedance values, more power is reflected back towards the transmitter than that is transmitted out through the antenna. The attenuator helps avoid this by balancing the impedance in the circuit. But, adding an attenuator also adds noise to the circuit. So, the attenuator should be carefully chosen so that there is a trade-off between the added noise and the impedance balancing capability. The attenuator chosen in this design is VAT-3+, which has a frequency range of up to 6000MHz. Measurements using the RF analyzer have shown that at the operating frequency of 2.4GHz, the attenuator attenuates 3.3dBm RF power.

An amplifier is a device which uses active elements like transistors to increase the power of a signal by a factor called the amplifier gain. The output of an amplifier has the same shape and frequency, but a higher amplitude than the input. The amplifier used in this circuit is an RF power amplifier, which converts the low power Radio Frequency (RF) signal into a high power signal required to drive the transmitting antenna. Such an amplifier has high efficiency, high gain and optimum heat dissipation. The power amplifier used in this design is ZX60-272LN+ with a frequency range of 2300-2700MHz. It has been tested using a series spectrum analyzer to show an increase of 12dBm RF power.

4.2.1.4. Splitter

The power splitter is a passive device that couples a part of the electromagnetic power in a transmission line to a port, so that the signal can be used in another circuit. In this circuit, the power splitter sends half of the total power to the transmitting antenna, and the rest to a mixer that compares this signal to the received signal. The splitter used in this design is ZX10-2-42-S+ with a frequency range of 1900-4200MHz. It has an input port and two output ports. It has been tested using the series spectrum analyzer by connecting an input signal of -8.3dBm power at the input and an attenuator at one output. The power at the second output is found to be -16.9dBm, a decrease in power by half.

4.2.2. Receive circuit

4.2.2.1. Low Noise Amplifier

The signal received by the receiver antenna is first amplified using the Low Noise Amplifier (LNA). The LNA used in this design is the same as the power amplifier ZX60-272LN+.

4.2.2.2. Mixer

The mixer has two inputs – one from transmission circuit, i.e., a part of the transmitted EM wave from the power splitter, and the other from the receiver antenna. Both these inputs being sinusoidal, their multiplication gives the phase difference between the transmitted and received waves. Consider the following equations for the transmitted and received waveforms:

Transmitted: $T = K_1 \cos(\omega t + \varphi)$ (4.19)

Received: $R = K2 \cos(\omega t + \varphi + \varphi_d)$ (4.20)

Where φ is the wavelength of the transmitted wave and φ_d is the delay in the phase as the transmitted wave strikes the target. The multiplication of these two sinusoidal waveforms gives a DC output $\cos(\varphi_d)$. This DC value is then amplified and filtered using a Low Pass Filter (LPF). The mixer used in the present design is ZX05-43MH+ with a frequency range of 824-4200MHz.

4.2.2.3. Video amplifier

The video amplifier circuit consists of two stages - a gain stage and a Low Pass Filter (LPF) stage. The gain stage amplifies the signal obtained from the mixer and the LPF attenuates the part of signal with frequency more than 15KHz. A quad-opamp MAX414CPD+ is used for both amplification and low pass filtering. A screenshot of simulation in Multisim for the video amplifier circuit is shown in figure 3.6.

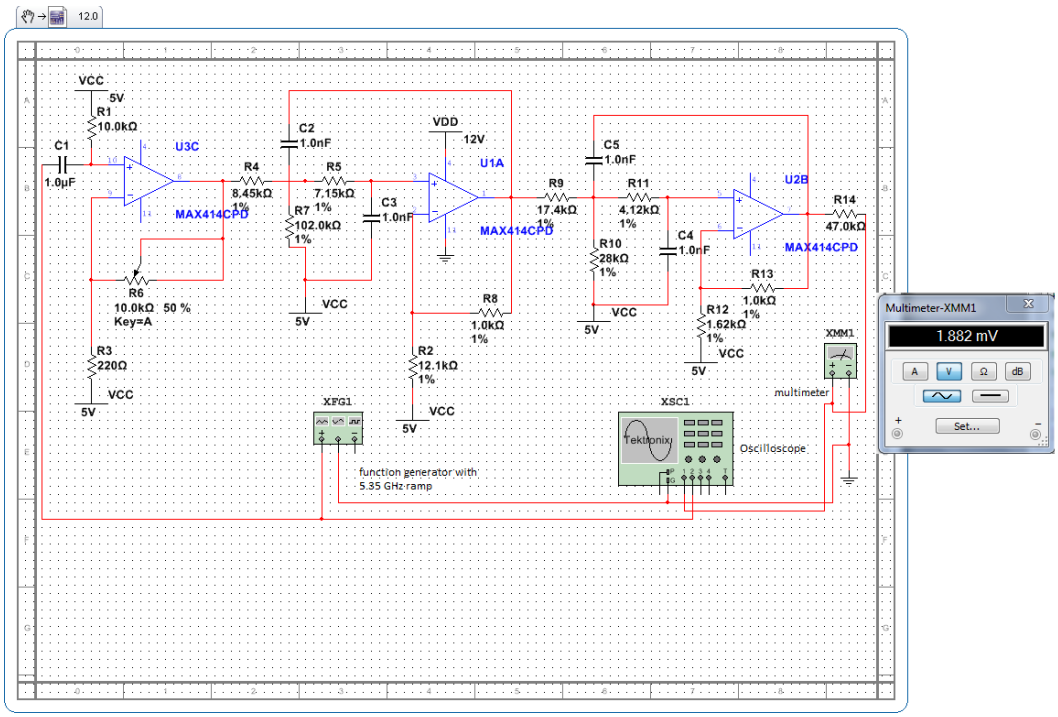

Figure 4.6: Multisim simulation of Video Amplifier circuit

4.2.3. Antennas

Circular waveguide antennas made of tin are used in the present design, owing to easy availability, ease of design and cost-effectiveness. The transmitting and receiving

antennae are exactly similar and placed next to each other, so that together they mimic a single antenna that both transmits and receives the microwave signals. Two separate antennas are used to avoid coupling of incoming and outgoing signals. The dimensions of the antennas depend on the transmit frequency. The following equations are used to determine the antenna dimensions.

The antenna will work if its operating frequency 2.4GHz is greater than the TE11 mode cutoff frequency f_c.

$$f_c = \frac{2c}{2.61\ D} \tag{4.21}$$

Where c is the speed of light and D is the diameter of the antenna. From the above equation, the diameter D must be greater than 7.3cm. in this design, the antenna diameter is taken as 9.9cm.

Wavelength of the electromagnetic wave in the waveguide, i.e., guide wavelength

$$\lambda g = \frac{\lambda}{\sqrt{1-\frac{\lambda}{1.705D}^2}} \tag{4.22}$$

For a frequency of 2.4GHz, free space wavelength, λ = 12.5 cm. So, guide wavelength is λ_g = 18.5cm

Length of the cantenna is

$$L = 0.7\,\lambda_g = 13.3\text{cm} \tag{4.23}$$

Length of monopole wire inside the cantenna = $\lambda/4 \approx$ 3cm. Distance of monopole wire from the closed end of cantenna $\approx \lambda_g/4$ = 4.6cm. Figure 3.7 shows a diagrammatic representation of the antenna used.

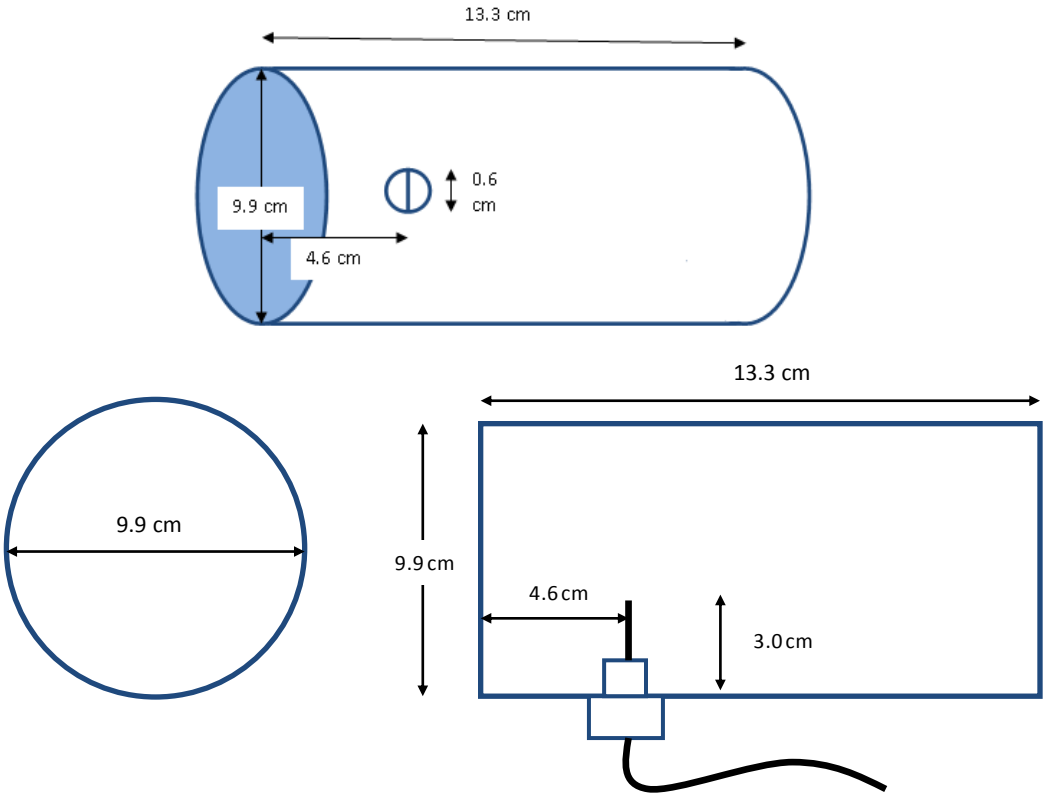

Figure 4.7: Dimensions of antennas

4.2.4. Collection of data using the radar system

After assembling the components, the output obtained from the video amplifier is recorded as an audio file (.wav format) by connecting an audio cable from the output to the audio input of a laptop. The audio file is then processed in MATLAB to give range and velocity profiles of objects moving in front of the radar system.

5. RESULTS AND DISCUSSIONS

This chapter presents the results obtained at each step explained in the methodology of SAR simulation. The validations and interpretations done on the obtained results are also provided. The input and output signals of the radar system built as a part of this project, are presented.

5.1. Simulation results

The simulation of RADARSAT-2 image of San Francisco area and the ALOS PALSAR image of Uttarakhand area are done in this study.

5.1.1. Simulation for RADARSAT-2

The required extents of ASTER and SRTM DEMs are first mosaicked and projected onto WGS84 UTM projection. ASTER and SRTM DEMs of San Francisco are shown in figures 5.1(b) and (b) respectively.

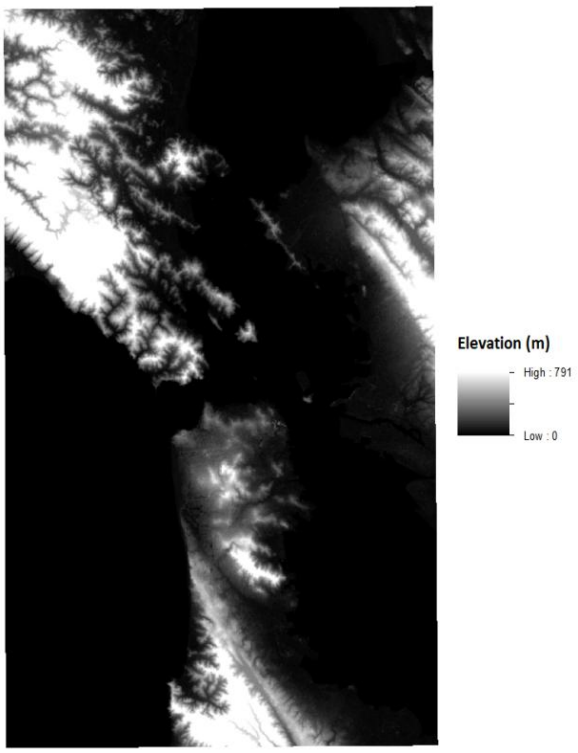

Figure 5.1(a): ASTER DEM of San Francisco

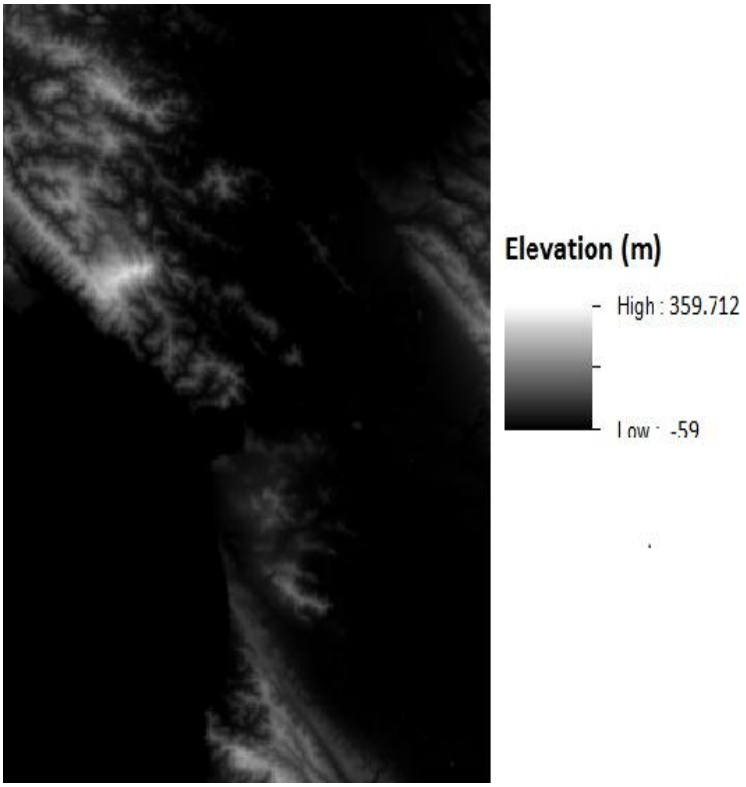

Figure 5.1(b): SRTM DEM of San Francisco

The latitude, longitude and elevation values are extracted from these DEMs and used in the simulation.

5.1.1.1. Satellite position and velocity vectors

RADARSAT's positions and velocities at five different points are extracted from the metadata and stored in a text file. Tables 5.1 and 5.2 show the positions and velocities of the satellite respectively.

Table 5.1: Positions of RADARSAT-2 (values are in m)

	X coordinate	Y coordinate	Z coordinate
Position 1	-3.432074E+06	-4.620627E+06	4.269915E+06
Position 2	-3.428909E+06	-4.608145E+06	4.285872E+06
Position 3	-3.425710E+06	-4.595627E+06	4.301796E+06
Position 4	-3.422480E+06	-4.583075E+06	4.317685E+06
Position 5	-3.419218E+06	-4.570486E+06	4.333539E+06

Table 5.2: Velocities of RADARSAT-2 (velocities are in m/s)

	X direction	Y direction	Z direction
position 1	1.159518E+03	4.588273E+03	5.880689E+03
position 2	1.171370E+03	4.601305E+03	5.868085E+03
position 3	1.183218E+03	4.614295E+03	5.855435E+03
position 4	1.195061E+03	4.627244E+03	5.842738E+03
position 5	1.206901E+03	4.640151E+03	5.829994E+03

5.1.1.2. Simulated images

The SAR image simulated from ASTER DEM and SRTM DEM are shown in figures 5.2(a) and 5.2(b) respectively.

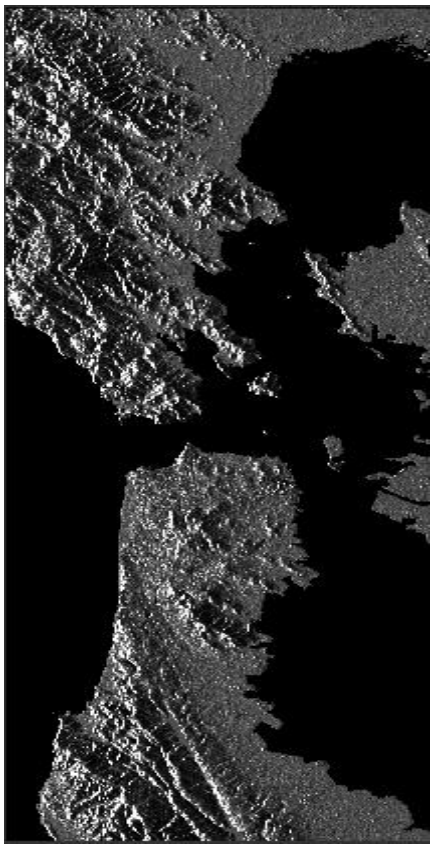

Figure 5.2(a): SAR image simulated from ASTER DEM

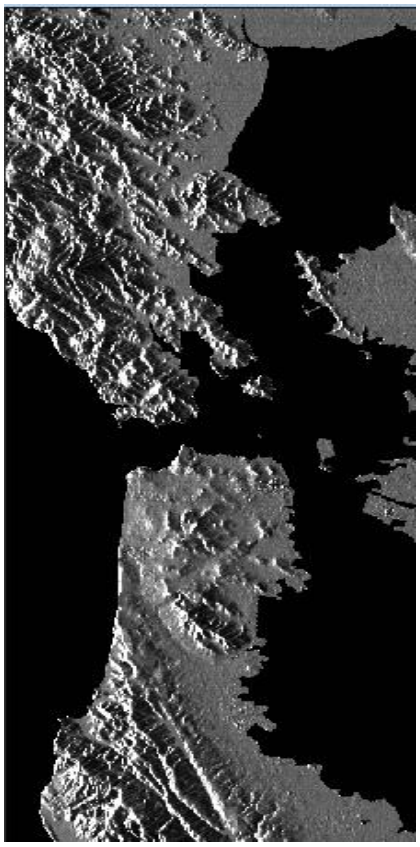

Figure 5.2(b): SAR image simulated from SRTM DEM

A comparison of the two images shows that the DEM of higher resolution, i.e., the ASTER DEM has produced a more detailed image. The undulations of the terrain are clearly seen when ASTER DEM is used. This shows how the 3D model of the target affects the output of the simulation algorithm.

The real SAR image of RADARSAT-2 for San Francisco area is shown in figure 5.3. the image shown is an intensity image in VH polarization.

Figure 5.3: Intensity image of RADARSAT-2 for San Francisco (VH polarization)

A comparison of the real SAR image with the simulated image shows that not all features appearing in the real SAR image are seen in the simulated image. This is because these features are not represented in the DEM used in the simulation. For example, the bridges seen in the real image do not appear in the simulated image.

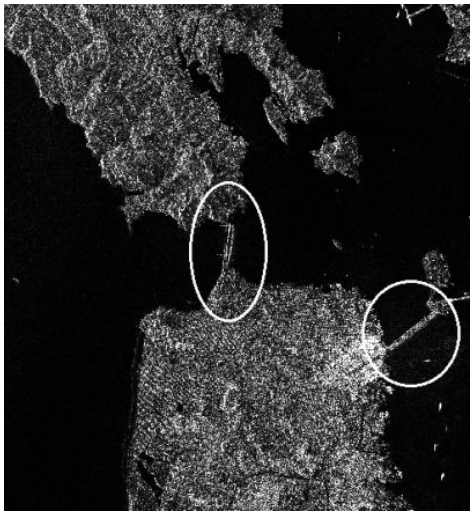

Figure 5.4(a): real SAR image showing bridges

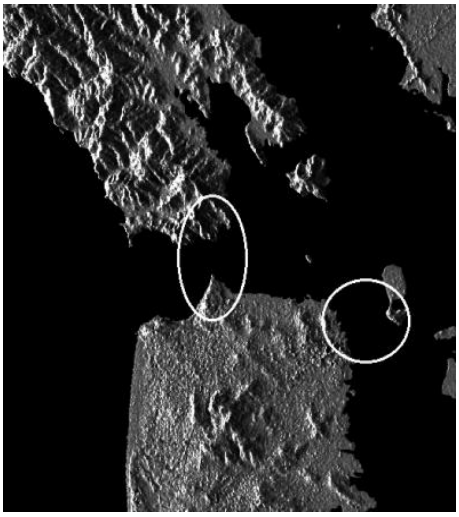

Figure 5.4(b): bridges absent in simulated image

There are also differences in the intensity values, as the surface properties of different objects on the surface have not been accounted for in the simulated image. Due to this drawback, the correlation between the actual image and the image simulated using ASTER DEM is 0.5975. Though the intensity values throughout the image do not match, the simulated image accurately shows the terrain structure. In general, this algorithm gives an accurate representation of the target geometry.

5.1.2. Simulation for ALOS PALSAR

The ALOS PALSAR image for Uttarakhand area is simulated using both ASTER and SRTM DEMs. Tiles of DEM are downloaded according to the area under consideration, mosaicked, and finally a subset of the exact area being simulated is made from the mosaicked DEM. The final ASTER DEM is given in figure 5.5 and SRTM DEM in figure 5.6.

Figure 5.5: ASTER DEM of Uttarakhand area

Figure 5.6: SRTM DEM of Uttarakhand area

5.1.2.1. Simulated images

The final simulated images for the ALOS PALSAR data using ASTER and SRTM DEMs are shown in figures 5.7 and 5.8 respectively.

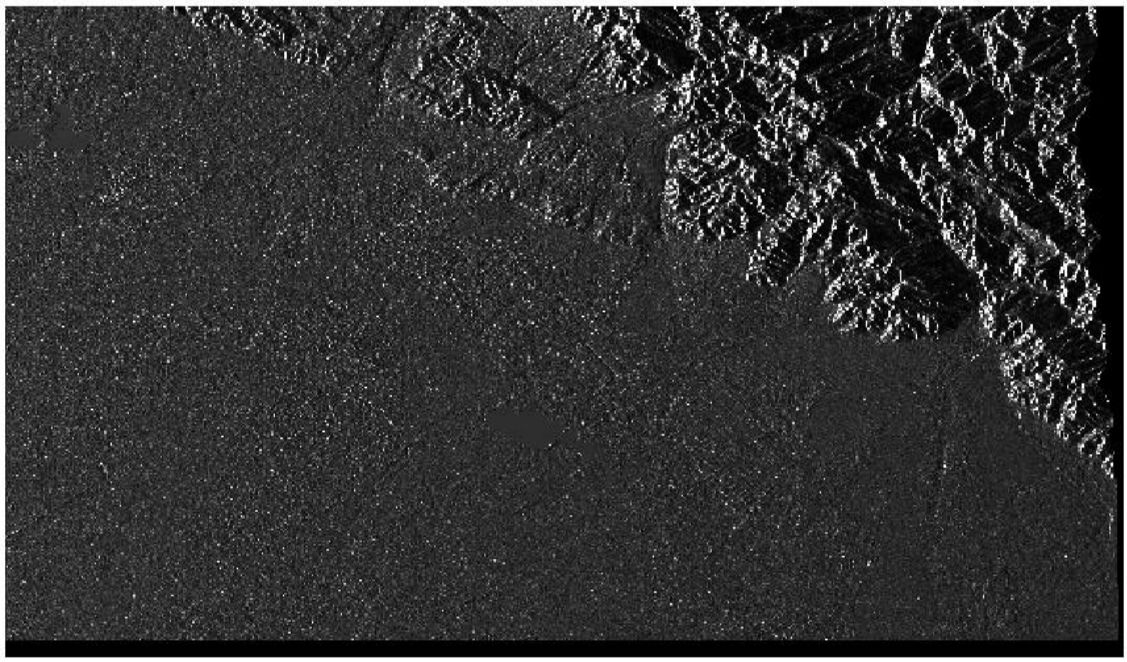

Figure 5.7: Simulated image based on ASTER DEM

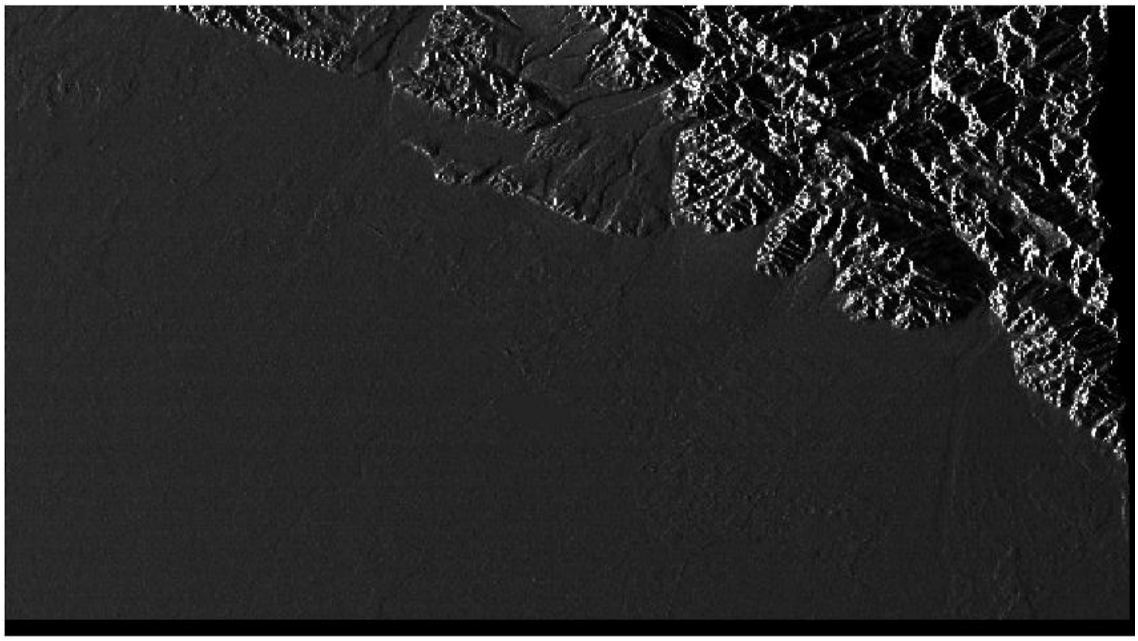

Figure 5.8: Simulated image based on SRTM DEM

A comparison of the simulated images with the real SAR image of ALOS PALSAR gives results similar to those observed in the case of RADARSAT-2 image. The correlation between the real PALSAR image and the image simulated using ASTER DEM is found to be 0.4856.

5.2. Outputs of radar system

The radar system is designed to work in S-band with an operating frequency of 2.4GHz. Signals at different modules of the system are tested. The final signal, i.e., the mixed signal of transmitted and received signals, is collected as an audio file and processed using MATLAB. The radar was operated in two modes - real aperture radar and synthetic aperture radar. The outputs for both the modes as well as the signals at various stages of the circuit are given in the following sections.

5.2.1. Output of the modulator

The modulator circuit of section (4.2.1.1) should give a triangular waveform of magnitude 2-3.2V, frequency 25Hz and an up-ramp time of 20ms. This is required to modulate the Voltage Controlled Oscillator in order to generate a signal in S-band frequency. The output of the modulator was connected to a Cathode Ray Oscilloscope (CRO) and was found to generate a perfect modulating signal of peak-to-peak voltage 2.36V, frequency 25Hz and time period 40ms (with a n up-ramp time period of 20ms). The CRO output is shown in figures 5.9(a) and (b).

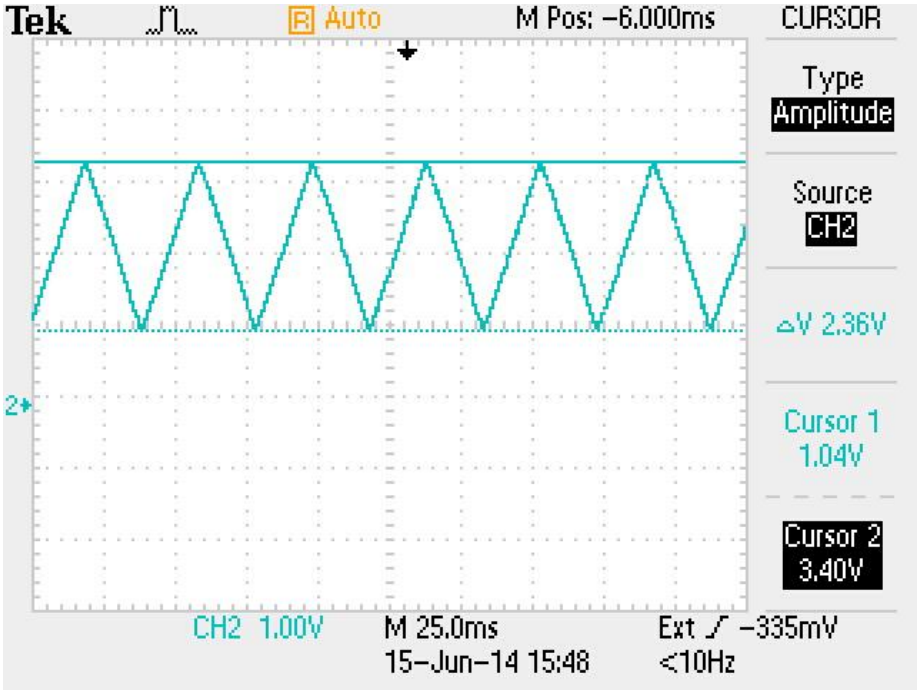

Figure 5.9(a): Modulator output showing a triangular waveform of amplitude 2.36V

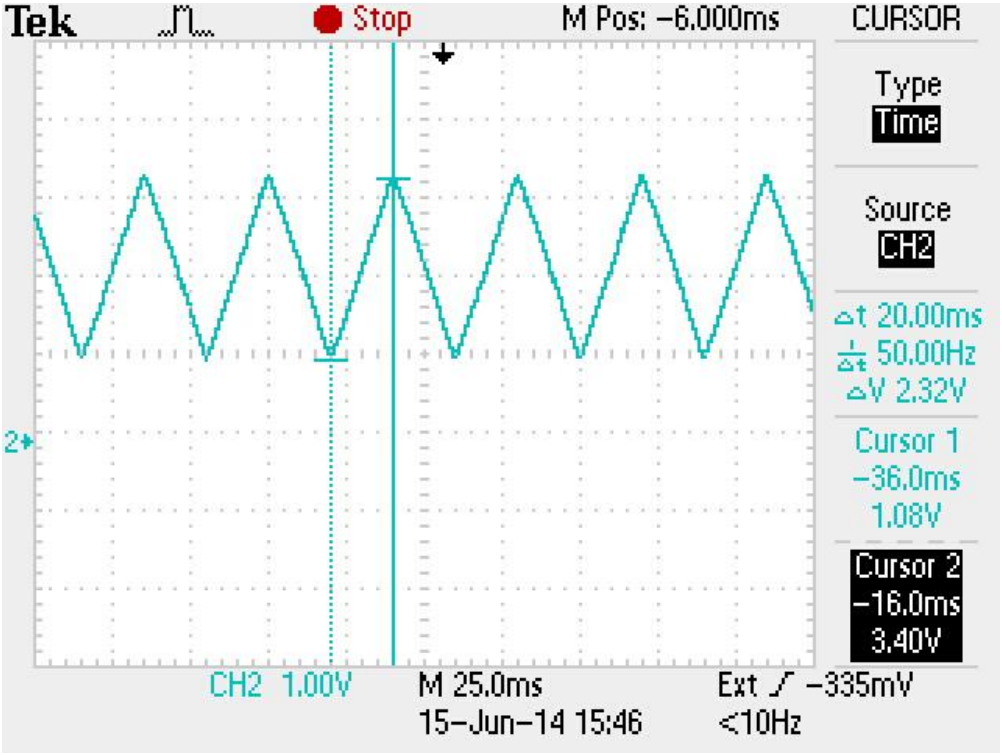

Figure 5.9(b): CRO screen showing a triangular wave with up-ramp time 20ms

5.2.2. Signal at the output of mixer

The transmitted and received RF signals are compared and a phase difference signal is generated in the mixer. The output of the mixer as seen in the CRO is given in figure 5.10.

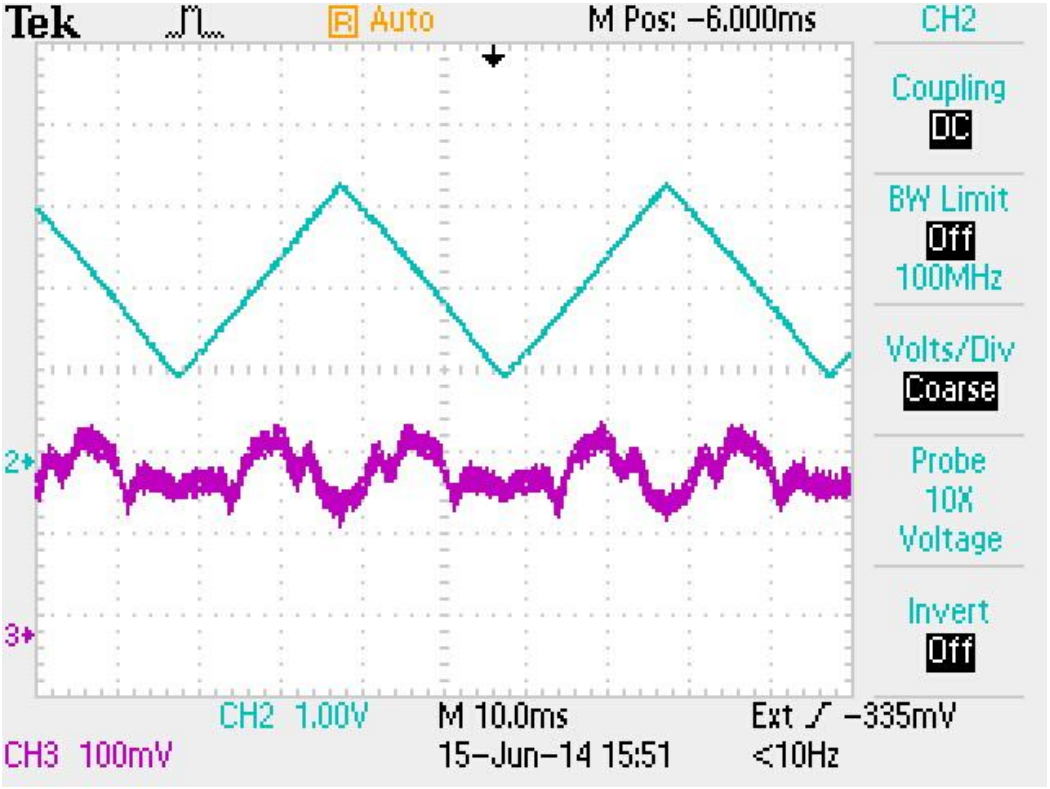

Figure 5.10: CRO screen showing modulating signal and mixer output. The signal in blue is the triangular output of modulator. The signal in purple is the mixer output, i.e., the phase difference signal of transmitted and received signals

The signal shown in purple colour in figure 4.8 is the output at the mixer when there is no moving target in the field of view of the radar system. It represents a scene where the transmitted radar signal is reflected back from the same objects which do not change either in position or in their orientation. Hence, the periodic signal.

5.2.3. Output of the video amplifier

The video amplifier has a gain stage and a Low Pass Filter (LPF) stage. The input to the gain stage is the signal from the mixer. After amplification in the gain stage, the signal goes through the LPF where the part of signal with frequency greater than 15 KHz is attenuated. The output of the video amplifier is shown in figure 5.11.

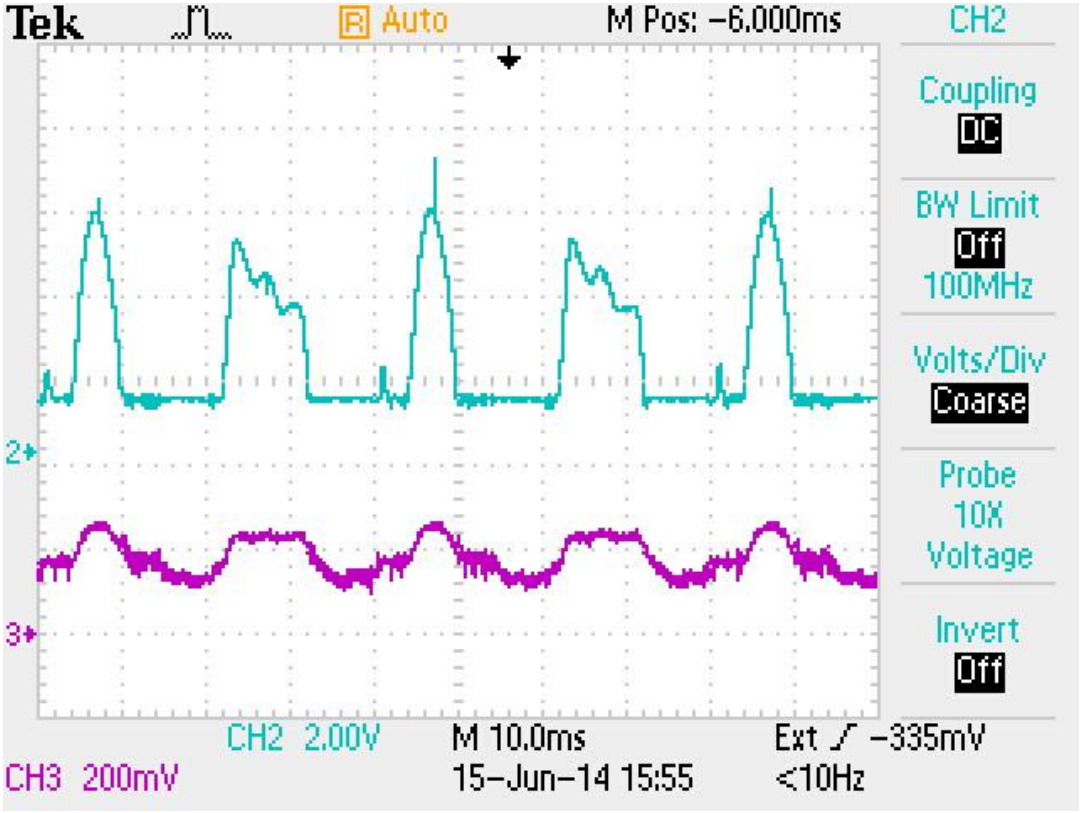

Figure 5.11: CRO screen showing outputs of mixer and video amplifier. The signal in purple is the mixer output, which is amplified in the video amplifier circuit to give the signal shown in blue.

5.2.4. Processing of radar output

The output of the video amplifier is recorded as an audio file (wav file) and processed in MATLAB. When the radar system is operated as a real aperture radar and used to image a moving target, a plot of time vs. range can plotted.

When the radar system is used as a Synthetic Aperture Radar (SAR), the audio file consists of the information of the position of sensor and the corresponding reflected signal at that position. This information is compressed in range and azimuth directions to generate an intensity image of the scene. The same audio file can also be used to create a time vs. range plot. A scene was created by placing three chairs at positions of different range and azimuth distances from the radar system. A diagrammatic representation of SAR implementation is shown in figure 5.12.

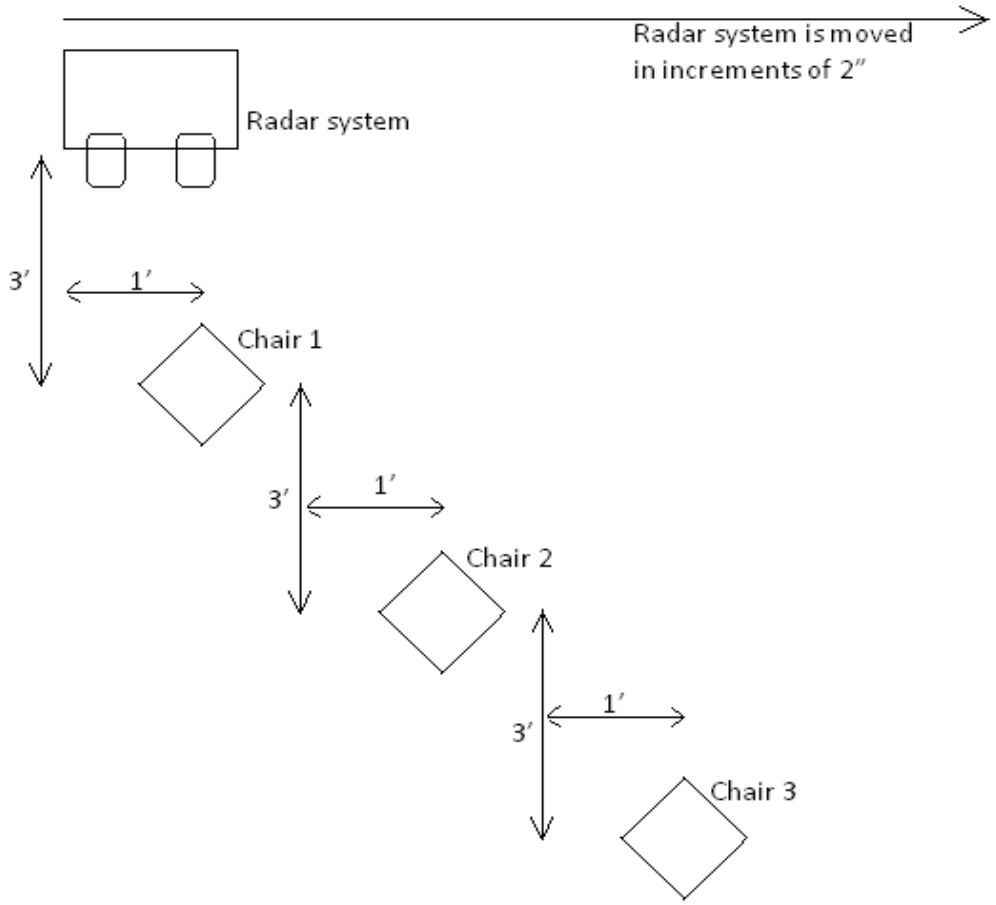

Figure 5.12: Image scene set for SAR implementation

The SAR image for the arrangement of figure 5.12 is given in figure 5.13.

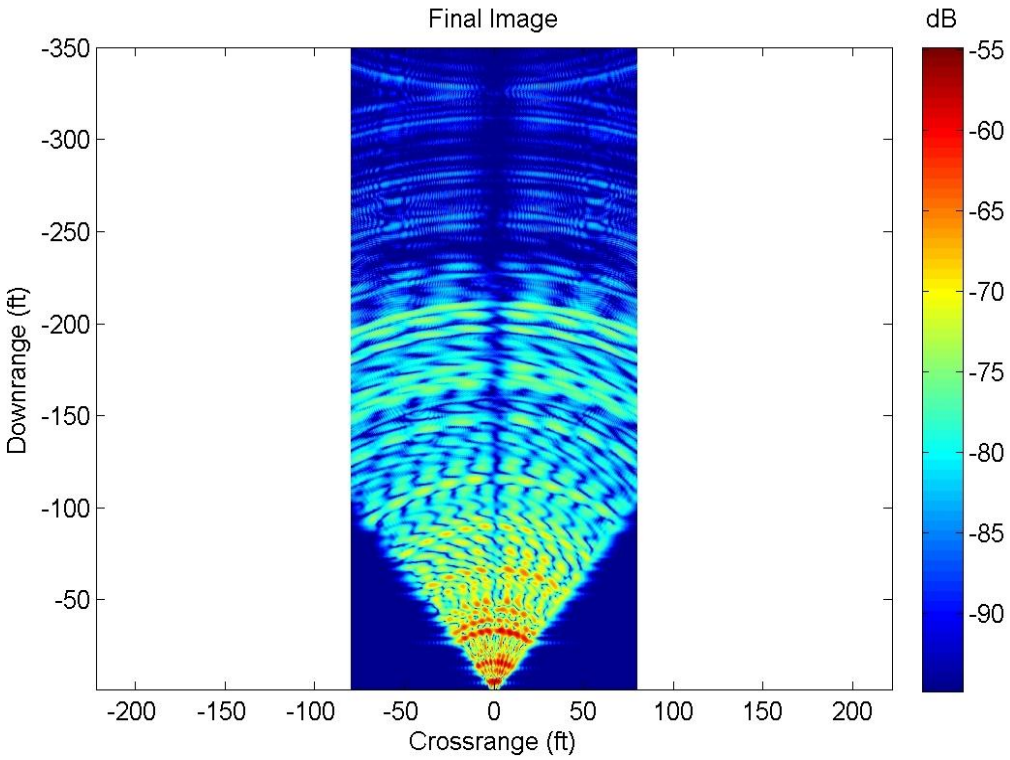

Figure 5.13: SAR intensity image

The SAR intensity image in figure 4.12 has a maximum range of 350ft. The colour bar at the right side of the image gives the signal-to-noise ratio in dB. The targets (i.e., the chairs) in the scene are placed up to a range of about 10ft. This is clearly seen in the SAR image as the bright orange-red patches corresponding to maximum signal-to-noise ratio. As the distance from the radar system increases, it can be seen that the signal-to-noise ratio decreases. This radar system is able to detect objects within a distance of about 200ft from the system.

A time vs. range plots of the same data at different sampling rates are shown in figures 5.14(a) and (b).

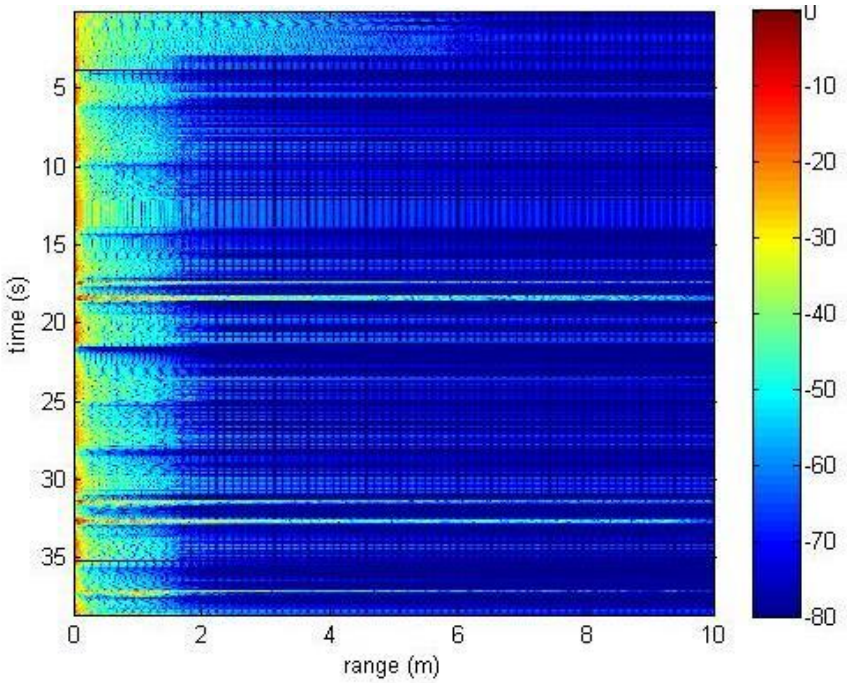

Figure 5.14(a): Range vs. time plot (sampling rate of 44100Hz)

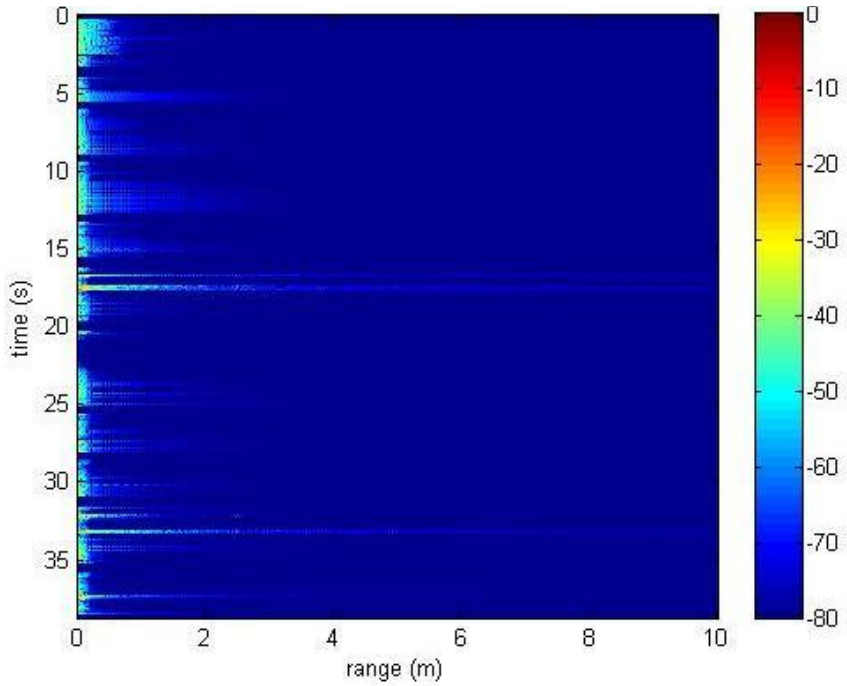

Figure 5.14(b): Range vs. time plot (sampling rate of 384000Hz)

As the radar system is moved in the azimuth direction, each of the chairs becomes a major scatterer one after the other. This can be observed from the three bright lines at time instants of approximately 18 seconds and 33 seconds in both the plots. With a higher sampling rate, the plot has lower noise and the time periods of imaging can also be visually differentiated from the plot.

6. CONCLUSIONS AND RECOMMENDATIONS

The main objective of this project is to simulate a SAR image from the target 3D model and SAR system parameters, and to design and operate a radar system that can be used to validate the simulation algorithm and make modifications to optimize it. The following sections present the conclusions on the basis of results obtained from the project and make recommendations with future scope in mind.

6.1. Conclusions

- The major inputs for SAR simulation can be categorized into two types: target parameters and sensor parameters. The target parameters include its geometry and orientation provided by its 3D model, and its surface characteristics like roughness and dielectric constant. In this project, the effects of geometry and orientation have been accounted for with the help of Digital Elevation Models, but the effects of surface characteristics have been approximated by using an empirically determined constant in the backscatter model.
- The SAR images have been simulated using DEMs of different resolutions. They show that the resolution of the 3D model used (DEM in this case) affects the quality of the final simulated SAR image. Though a model of higher resolution gives a more accurate SAR image than that of a lower resolution, it also uses greater memory and computational power. This was observed in the course of this project too. Simulation using ASTER DEM took a clearly larger amount of time and occupied more space in the memory than that using SRTM DEM. Hence, the choice of 3D model must be made depending on the application for which simulation technique is being used. For applications like target identification, a very detailed image is required and hence, a model of higher resolution must be used. For real-time applications, the details do not have as much importance as the fast availability of data. In such cases, a low resolution model must be used to save time and computational power.
- The correlation between the simulated and real SAR images is only about 60%. This is because the surface properties of the different features on the ground are not taken into account in the simulation algorithm. This leads to non-uniform differences in the backscatter values of different features. For instance, the Muhleman constant in the Muhleman's backscatter model is determined empirically for rocky surfaces. So, if the ground is predominantly rocky with no other major features, the algorithm gives better results. If, on the other hand, the area has different features like vegetation, urban structures, etc., the error in simulated output is greater.

- An elementary design of a radar system is implemented using low cost and easily available materials. The change in the received signal when an object is moved in front of the radar system has been observed using a Cathode Ray Oscilloscope (CRO). This same signal is compared with the transmitted signal to get a phase difference signal. This difference signal is then used to plot phase vs. time graphs and images. Though the system needs to be optimized further, the results obtained are satisfactory and as predicted.
- The radar system has been implemented as a Synthetic Aperture Radar and has given expected outputs. The output is shown as a plot of crossrange (azimuth) vs. downrange, with a maximum downrange of 350ft. But, the range up to which the system can sense targets is around 100ft. As the system components have not been optimized, the range and resolutions are poor.

6.2. Recommendations

The difficulty in the interpretation of SAR images has always been a disadvantage for microwave remote sensing. Despite the many advantages of microwaves like all-weather capability, moisture sensitivity and high resolution capability through SAR implementation, microwave remote sensing has not seen many users because of the experience and expertise required to use the microwave data. SAR images are sometimes confusing even to those who are experienced at handling them, as so many factors affect how the microwaves are reflected from the targets. The technique of SAR simulation helps in the study of SAR image interpretation and what factors affect the object signatures in a SAR image. The study of simulation images can help in familiarizing users with the concept of microwave remote sensing, thus resulting in an increase in its usage.

This project shows how easily available materials can be used to build a radar system that can also function as a Synthetic Aperture Radar. Such systems are extremely useful when real time data is required or when field experiments need to be carried out. Once the processing of the data collected is mastered, any simulation algorithm can be tested with fairly high accuracy.

6.3. Future scope

There are certain limitations of this study which can be overcome through further research on the topic. The limitations and future work are given below:

- An attempt can be made to increase the scope of this algorithm by using a better backscatter model. The simulation algorithm used in this study has given fairly good results for Digital Elevation Models, but uses the Muhleman's backscatter model to calculate the backscattered intensity. This model cannot be used at

high resolutions, as it can't account for changes in the surface properties of different objects. So, to simulate images of high resolutions, a model which accounts for the dependency of backscattered intensity on target surface characteristics must be used.

- Now that the algorithm works for Digital Elevation Models, it can be extended to 3D models of individual objects to study how geometry and composition of a target affect SAR images.
- The SAR system's resolution can be further increased by using metal of higher conductivity for the antennas, and providing the system some protection from outside noise and interference.
- Once the system is optimized and is able to give an accurate range of targets, it can be calibrated against standard materials whose reflection characteristics are known.
- The simulation algorithm can be used to generate SAR images of individual objects, but their 3D models must first be created. These images can then be validated using the images generated by the SAR system.

REFERENCES

Auer, S., S. Hinz, and R. Bamler. 2010. "Ray-Tracing Simulation Techniques for Understanding High-Resolution SAR Images." *IEEE Transactions on Geoscience and Remote Sensing* 48 (3): 1445–56. doi:10.1109/TGRS.2009.2029339.

Auer, Stefan J. 2011. "3D Synthetic Aperture Radar Simulation for Interpreting Complex Urban Reflection Scenarios". PhD, Germany: Technischen Universitat Munchen.

Balz, Timo. 2004. "SAR Simulation Based Change Detection with High-resolution SAR Images in Urban Environments." *IAPRS Vol. 35, Part B*.

Balz, Timo, and Norbert Haala. 2006. "Improved Real-time SAR Simulation in Urban Areas." In *International Geoscience and Remote Sensing Symposium (IGARSS)*, 3631–34.

Cakir, Gonca, Mustafa Cakir, and Levent Sevgi. 2008. "Radar Cross Section (RCS) Modeling and Simulation, Part 2: a Novel FDTD-based RCS Prediction Virtual Tool for the Resonance Regime." *Antennas and Propagation Magazine, IEEE* 50 (2): 81–94.

Çakir, Gonca, and Levent Sevgi.2010. "Radar cross-section (RCS) analysis of high frequency surface wave radar targets." *Turkish Journal of Electrical Engineering & Computer Sciences* 18.3: 457-468.

Çakır, Mustafa, Gonca Çakır, and Levent Sevgi. 2014. "PARALLEL FDTD-BASED RADAR CROSS SECTION SIMULATIONS." Accessed June 10.

Chang, Y.-L., C.-Y. Chiang, and K.-S. Chen. 2011. "SAR IMAGE SIMULATION WITH APPLICATION TO TARGET RECOGNITION." *Progress In Electromagnetics Research* 119.

Chiu, Shen, and Chuck Livingstone. 2005. "A Comparison of Displaced Phase Centre Antenna and Along-track Interferometry Techniques for RADARSAT-2 Ground Moving Target Indication." *Canadian Journal of Remote Sensing* 31 (1): 37–51.

Curlander, John C., and Robert N. McDonough. *Synthetic aperture radar*. Vol. 199. No. 1. New York: Wiley, 1991.

Dogan, Ozan, and Mesut Kartal.2010 "Time domain SAR raw data simulation of distributed targets." *EURASIP Journal on Advances in Signal Processing* 2010: 100.

Eng, M., and René Schwarz. 2013. "Keplerian Orbit Elements-→ Cartesian State Vectors." https://downloads.rene-schwarz.com/download/M001-Keplerian_Orbit_Elements_to_Cartesian_State_Vectors.pdf.

Franceschetti, Giorgio, Maurizio Migliaccio, Daniele Riccio, and Gilda Schirinzi. 1992. "SARAS: A Synthetic Aperture Radar (SAR) Raw Signal Simulator." *IEEE TRANSACTIONS ON GEOSCIENCE AND REMOTE SENSING* 30 (January).

Franceschetti, G., Migliaccio, M., Riccio, Daniele.1995. "The SAR simulation: an overview," *Geoscience and Remote Sensing Symposium, 1995. IGARSS '95. 'Quantitative Remote Sensing for Science and Applications', International* , vol.3, no., pp.2283,2285 vol.3, 10-14 Jul1995

Franceschetti, Giorgio, Raffaella Guida, Antonio Iodice, Daniele Riccio, Giuseppe Ruello, and Uwe Stilla. 2007. "Simulation Tools for Interpretation of High Resolution SAR Images of Urban Areas." In *Urban Remote Sensing Joint Event, 2007*, 1–5. IEEE.

Hammer, Horst, Timo Balz, Erich Cadario, Uwe Soergel, Ulrich Thoennessen, and Uwe Stilla. 2008. "Comparison of SAR Simulation Concepts for the Analysis of High-resolution SAR Data." In *Synthetic Aperture Radar (EUSAR), 2008 7th European Conference On*, 1–4. VDE.

Japan Aerospace Exploration Agency. 2009. "ALOS/PALSAR Level 1.1/1.5 Format Description". Japan Aerospace Exploration Agency.

Jensen, Henrik W. 2001. *Realistic Image Synthesis Using Photon Mapping*. Massachusetts: A K Peters.

Ligas, Marcin, and Piotr Banasik. 2011. "Conversion Between Cartesian and Geodetic Coordinates on a Rotational Ellipsoid by Solving a System of Nonlinear Equations." *Geodesy and Cartography* 60 (2): 145–59.

Liu, Hongxing, Zhiyuan Zhao, and Kenneth C. Jezek. 2004. "Correction of Positional Errors and Geometric Distortions in Topographic Maps and DEMs Using Rigorous

SAR Simulation Technique." *Photogrammetric Engineering and Remote Sensing* 70 (9): 1031–42.

Mishra, D.K. (2001). *Radio-Frequency and Microwave Communication Circuits: Analysis and Design*: John Wiley & Sons, Inc.

"NORAD Two-Line Element Sets Current Data." [Online]. Available: http://www.celestrak.com/NORAD/elements/ . [Accessed: 16-Dec-2013].

Schneider, John B. 2010. "Understanding the Finite-difference Time-domain Method." *Scholl of Electrical Engineering and Computer Science Washington State University.– URL: Http://www. Eecs. Wsu. Edu/~ Schneidj/ufdtd/(request Data: 29.11. 2012).*

Slade, Bob. 2013. "RADARSAT-2 Product Description". MacDonald, Dettwiler and Associates Ltd.

Storvold, Rune, K. A. Hogda, E. Malnes, and I. Lauknes. 2004. "SAR Firn Line Detection and Correlation to Glacial Mass Balance Svartisen Glacier, Northern Norway." In Salzburg, Austria.

Uluisik, Cagatay, Gonca Cakir, Mustafa Cakir, and Levent Sevgi. 2008. "Radar Cross Section (RCS) Modeling and Simulation, Part 1: a Tutorial Review of Definitions, Strategies, and Canonical Examples." *Antennas and Propagation Magazine, IEEE* 50 (1): 115–26.

Wolff, Christian. 1996. "Radartutorial.eu" [Online]. Available: http://www.radartutorial.eu/. [Accessed: 24-Feb-2014].

APPENDIX 1

Codes used for simulation

Extraction of information from satellite metadata using Python:

```
import os
import numpy
os.chdir('D:/Kimeera')
import lxml
from lxml import etree
tree = etree.parse('product.xml')
root = tree.getroot()
xpos = []
ypos = []
zpos = []
for x in
root.iter(tag='{http://www.rsi.ca/rs2/prod/xml/schemas}xPosit
ion'):
    xpos.append(x.text)
for y in
root.iter(tag='{http://www.rsi.ca/rs2/prod/xml/schemas}yPosit
ion'):
    ypos.append(y.text)
for z in
root.iter(tag='{http://www.rsi.ca/rs2/prod/xml/schemas}zPosit
ion'):
    zpos.append(z.text)
X = numpy.zeros((5,1))
Y = numpy.zeros((5,1))
Z = numpy.zeros((5,1))
for i in range (5):
    X[i]=xpos[i]
for j in range (5):
    Y[j]=ypos[j]
for k in range (5):
    Z[k]=zpos[k]
numpy.savetxt('xposition.txt',X,delimiter='\t',newline='\n')
numpy.savetxt('yposition.txt',Y,delimiter='\t',newline='\n')
numpy.savetxt('zposition.txt',Z,delimiter='\t',newline='\n')
```

MATLAB program for the calculation of image row and column numbers:

```
t = load('test1_22.txt', '-ascii');
P = load('aster_demOP.txt', '-ascii');
```

```
S = [56.55 -116 -7637 4.237e6; 120.6 -164.9 -1.997e4 3.86e6; -165.6
136.4 2.538e4 4.302e6];
%n = size(t);
toff = 14.898;
dt = 6.9507e-4;
Roff = 8.881938261133428e5;
dR = 4.73307896;
for i=1:200000
    row(i,1) = (t(i,1)-toff)/dt;
    T4 = conv((S(1,:)-[0 0 0 P(i,1)]),(S(1,:)-[0 0 0
P(i,1)]))+conv((S(2,:)-[0 0 0 P(i,2)]),(S(2,:)-[0 0 0
P(i,2)]))+conv((S(3,:)-[0 0 0 P(i,3)]),(S(3,:)-[0 0 0 P(i,3)]));
    R =
sqrt(T4(1,1)*t(i,1)^6+T4(1,2)*t(i,1)^5+T4(1,3)*t(i,1)^4+T4(1,4)*t(i,
1)^3+T4(1,5)*t(i,1)^2+T4(1,6)*t(i,1)+T4(1,7));
    col(i,1) = (R-Roff)/dR;
end
dlmwrite('rows_12.txt',row, 'delimiter','\t','precision',12);
dlmwrite('columns_15.txt',col, 'delimiter','\t','precision',15);
```

MATLAB program for the calculation of backscatter values:

```
inci = load('incidence.txt', '-ascii');
n = size(inci);
sig=zeros(n(1,1),n(1,2));
for i=1:n(1,1)
    for j=1:n(1,2)
        sig(i,j) =
log10(0.0133*cos(inci(i,j))/(sin(inci(i,j))+0.1*cos(inci(i,j)))^3);
    end
end
dlmwrite('sigma.txt',sig, '\t');
```

APPENDIX 2

Electrical characteristics of components used:

Voltage Controlled Oscillator:

Table 1: Electrical specifications of VCO ZX95-2536C+

Electrical Specifications

MODEL NO.	FREQ. (MHz)		POWER OUTPUT (dBm)	PHASE NOISE dBc/Hz SSB at offset frequencies,kHz				TUNING					NON HARMONIC SPURIOUS (dBc)	HARMONICS (dBc)		PULLING pk-pk @12 dBr (MHz)	PUSHING (MHz/V)	DC OPERATING POWER	
				Typ.				VOLTAGE RANGE (V)		SENSI-TIVITY (MHz/V)	PORT CAP (pF)	3 dB MODULATION BANDWIDTH (MHz)						Vcc (volts)	Current (mA)
	Min.	Max.	Typ.	1	10	100	1000	Min.	Max.	Typ.	Typ.	Typ.	Typ.	Typ.	Max.	Typ.	Typ.		Max.
ZX95-2536C+	2315	2536	+6	-75	-105	-128	-148	0.5	5	57-77	13.6	70	-90	-18	-10	2.5	2.5	5	45

Power Amplifier:

Table 2: Electrical characteristics of Power Amplifier ZX60-272LN+

Electrical Specifications at 25°C

Parameter	Condition (MHz)	Min.	Typ.	Max.	Units
Frequency Range		2300		2700	MHz
Noise Figure	2300-2700		0.8	1.1	dB
Gain	2300-2700	11.5	14.0		dB
Gain Flatness	2300-2700		± 0.55	± 1.1	dB
Output Power at 1dB compression	2300-2700	16.0	18.5		dBm
Output third order intercept point (OIP3)	2300-2700		31.5		dBm
Input VSWR	2300-2700		1.2		:1
Output VSWR	2300-2700		1.6		:1
Active Directivity	2300-2700		7		dB
DC Supply Voltage			5.0		V
Supply Current			55	70	mA

Attenuator:

Table 3: Electrical specifications and performance data of attenuator VAT-3+

FREQ. RANGE (MHz)	ATTENUATION * (dB) Flatness **					VSWR (:1)					MAX. INPUT POWER (W)
		DC-3 GHz	3-5 GHz	5-6 GHz	DC-6 GHz	DC-3 GHz		3-5 GHz		5-6 GHz	
f_L-f_U	Nom.	Typ.	Typ.	Typ.	Typ.	Typ.	Max.	Typ.	Max.	Typ.	
DC-6000	3±0.3	0.20	0.15	0.15	0.45	1.05	1.20	1.15	1.40	1.40	1.0

Frequency (MHz)	Attenuation (dB)	VSWR (:1)
0.03	3.02	1.00
50.00	3.00	1.00
100.00	3.00	1.01
500.00	3.05	1.03
1000.00	3.10	1.05
2000.00	3.19	1.05
3000.00	3.31	1.03
4000.00	3.43	1.10
5000.00	3.58	1.24
6000.00	3.81	1.39

Splitter:

Table 4: Electrical specifications and performance data of splitter ZX-10-2-42+

FREQ. RANGE (MHz)	ISOLATION (dB)		INSERTION LOSS (dB) ABOVE 3.0 dB		PHASE UNBALANCE (Degrees)	AMPLITUDE UNBALANCE (dB)
f_L-f_U	Typ.	Min	Typ.	Max.	Max.	Max.
1900-4200	23	10	0.2	1.0	3.0	0.3
2600-3400	23	17	0.2	0.5	2.0	0.3

Frequency (MHz)	Insertion Loss (dB)		Amplitude Unbalance (dB)	Isolation (dB)	Phase Unbalance (deg.)	VSWR S	VSWR 1	VSWR 2
	S-1	S-2						
1900.00	3.45	3.45	0.00	12.33	0.70	1.79	1.08	1.07
2040.00	3.42	3.44	0.02	13.42	0.71	1.71	1.09	1.08
2180.00	3.37	3.36	0.01	14.64	0.74	1.62	1.10	1.09
2460.00	3.26	3.26	0.01	17.92	0.91	1.47	1.09	1.08
2600.00	3.19	3.19	0.00	20.16	1.05	1.39	1.08	1.08
2760.00	3.19	3.18	0.01	23.66	1.02	1.26	1.05	1.05
2920.00	3.10	3.12	0.02	27.75	1.18	1.14	1.02	1.03
3240.00	3.11	3.11	0.00	23.53	1.50	1.07	1.03	1.02
3400.00	3.13	3.16	0.03	20.10	1.54	1.19	1.05	1.10
3540.00	3.23	3.27	0.04	17.91	1.30	1.31	1.07	1.05
3680.00	3.26	3.29	0.03	16.12	1.55	1.40	1.07	1.06
3820.00	3.31	3.36	0.05	14.58	1.52	1.51	1.09	1.08
4100.00	3.48	3.52	0.03	12.21	1.48	1.78	1.15	1.15
4150.00	3.54	3.58	0.04	11.90	1.37	1.83	1.16	1.16
4200.00	3.52	3.55	0.03	11.51	1.50	1.87	1.17	1.18

Mixer:

Table 5: Electrical specifications and performance data of mixer ZX05-43MH+

FREQUENCY (MHz)		CONVERSION LOSS* (dB)			LO-RF ISOLATION (dB)		LO-IF ISOLATION (dB)		IP3 at center band (dBm)
LO/RF f_L-f_U	IF	Typ.	σ	Max.	Typ.	Min.	Typ.	Min.	Typ.
824-4200	DC-1500								
824-2500		6.3	0.1	8.6	37	28	24	7	20
2500-4200		5.7	0.1	9.8	30	22	20	11	22

Frequency (MHz)		Conversion Loss (dB)	Isolation L-R (dB)	Isolation L-I (dB)	VSWR RF Port (:1)	VSWR LO Port (:1)
RF	LO	LO +13dBm	LO +13dBm	LO +13dBm	LO +13dBm	LO +13dBm
810.00	840.00	7.06	38.11	22.81	2.08	8.55
1010.00	1040.00	6.43	43.16	26.73	2.83	2.44
1210.00	1240.00	5.83	41.09	30.74	3.45	1.27
1410.00	1440.00	5.82	34.44	34.76	3.53	1.16
1610.00	1640.00	5.70	33.13	29.18	3.12	1.61
1810.00	1840.00	6.00	35.10	19.67	3.21	1.77
2010.00	2040.00	5.93	33.76	11.58	3.28	1.62
2210.00	2240.00	5.94	34.33	11.64	3.33	1.85
2410.00	2440.00	5.12	31.89	14.42	2.18	2.27
2610.00	2640.00	5.44	31.05	17.41	2.43	2.37
2810.00	2840.00	5.15	29.56	19.09	1.88	1.72
3010.00	3040.00	4.63	27.17	21.48	1.70	1.64
3210.00	3240.00	4.96	25.87	25.21	1.92	1.37
3410.00	3440.00	5.46	25.97	24.10	2.11	1.34
3610.00	3640.00	6.47	24.80	20.53	3.34	1.88
3810.00	3840.00	6.88	25.65	18.07	3.76	2.58
4010.00	4040.00	7.75	26.66	17.01	5.03	3.83
4110.00	4140.00	7.74	26.80	15.46	5.14	4.62
4150.00	4180.00	7.92	26.85	15.58	5.44	4.84
4210.00	4240.00	7.83	26.88	15.04	5.07	5.28

Function generator XR2206:

Table 6: Electrical specifications of XR2206

Parameters	XR-2206M/P			XR-2206CP/D			Units	Conditions
	Min.	Typ.	Max.	Min.	Typ.	Max.		
General Characteristics								
Single Supply Voltage	**10**		**26**	**10**		**26**	V	
Split-Supply Voltage	±5		±13	±5		±13	V	
Supply Current		12	**17**		14	20	mA	$R_1 \geq 10k\Omega$
Oscillator Section								
Max. Operating Frequency	**0.5**	1		0.5	1		MHz	**C = 1000pF, R_1 = 1kΩ**
Lowest Practical Frequency		0.01			0.01		Hz	C = 50µF, R_1 = 2MΩ
Frequency Accuracy		±1	±4		±2		% of f_0	$f_0 = 1/R_1C$
Temperature Stability Frequency		±10	±50		±20		ppm/°C	$0°C \leq T_A \leq 70°C$ $R_1 = R_2 = 20k\Omega$
Sine Wave Amplitude Stability[2]		4800			4800		ppm/°C	
Supply Sensitivity		0.01	**0.1**		0.01		%/V	V_{LOW} = 10V, V_{HIGH} = 20V, $R_1 = R_2 = 20k\Omega$
Sweep Range	1000:1	2000:1			2000:1		$f_H = f_L$	f_H @ R_1 = 1kΩ f_L @ R_1 = 2MΩ
Sweep Linearity								
10:1 Sweep		2			2		%	f_L = 1kHz, f_H = 10kHz
1000:1 Sweep		8			8		%	f_L = 100Hz, f_H = 100kHz
FM Distortion		0.1			0.1		%	±10% Deviation
Recommended Timing Components								
Timing Capacitor: C	**0.001**		100	0.001		100	µF	*Figure 5*
Timing Resistors: R_1 & R_2	**1**		2000	1		2000	kΩ	
Triangle Sine Wave Output[1]								*Figure 3*
Triangle Amplitude		160			160		mV/kΩ	*Figure 2*, S_1 Open
Sine Wave Amplitude	**40**	60	80		60		mV/kΩ	*Figure 2*, S_1 Closed
Max. Output Swing		6			6		Vp-p	
Output Impedance		600			600		Ω	
Triangle Linearity		1			1		%	
Amplitude Stability		0.5			0.5		dB	For 1000:1 Sweep
Sine Wave Distortion								
Without Adjustment		2.5			2.5		%	R_1 = 30kΩ
With Adjustment		0.4	**1.0**		0.5	1.5	%	See *Figure 7* and *Figure 8*